The Oligo – Miocene Volcanism of the Red Sea Rift Valley: Petrology and geochemistry of the volcanic activity in the Northwestern Sinai, Egypt

Hatem M. El-Desoky[1] and Ramadan E. El-shafey[2]

[1]Department of Geology, Faculty of Science, Al-Azhar University, Cairo, Egypt
[2]Geologist at El-Arish Cement Company (ArCC), Sinai, Egypt
hatem_eldesoky@yahoo.com

Abstract: The Oligo-Miocene Volcanism of the Red Sea Rift Valley at Al-Hemmah-Resan Ikteifa district are characterized by hills and sheets outcrops of "within plate" tholeiitic alkali basalt and dolerite. Al-Hemmah and Resan Ikteifa volcanic rocks are formed mainly of non-porphyritic olivine dolerite together with some porphyritic olivine basalts. Geochemically the basalt and dolerite are alkaline to subalkaline. The alkaline character is confirmed by the appearance of nepheline in the norms. Various discrimination diagrams confirm the "within plate" character of basalt and dolerite. They are derived from subcontinental lithospheric enriched mantle, and rule out asthenospheric mantle source in true continental rift environments, are good agreement between the studied basaltic samples and N-MRB and E-MORB, affected by crustal contamination. The tholeiitic nature is evident from Nb-Zr-Y plot. The basalts with normative nepheline are generally enriched in alkalis. These rocks relatively enriched of Zn, Zr and Cr which characterizes the tholeiitic rocks.

1. Introduction

The Red Sea Rift in the Oligocene is the main tectonic structures in the north Egypt. It is a continental plate boundary separating the Arabian Plate from the Sinai Sub-Plate, originating at the Red Sea Rift in the south and terminating after approximately 1200 km to the north at the continental collision zone of the Taurus Zagros orogenic belt (**Garfunkel, 1981**). The northern part of the Red Sea is in the late stage of continental rifting (**Cochran et al., 1986**), whereas the southern part exhibits already organized sea floor spreading for the past 5 Ma (**Röser, 1975**); the central part is in a transition stage from rifting to drifting. This makes the Red Sea a unique place in the world to study the evolution from continental rifting to sea floor spreading. In the Miocene, about 20 Ma ago (**Courtillot et al., 1987**), a major change occurred in the Red Sea Rift.

The Oligo – Miocene Volcanism associated with Red Sea rifting at the north of the Egypt, is represented by the basalts and dolerites which constitute a distinct anorogenic igneous rift assemblage of widespread volcanic activity. The volcanism extending from Western Desert (Sixth of October, Tell El-Haddadine, Tell El-Zalaat, Gabal Qatrani, Gabal El-Hefhuf, Gabal Mindisha, El-Agoz, El-Bahr, Naqb Siwa-El-Quzzeih, Tibniya and El-Alawy El-Zurg), Eastern Desert (Naqb Ghul, Gabal Abu Treifiya, El-Yahmum, Gabal El-Nassuri, Gabal

Anqabia, Gabal Rawisat, and Abu Zaabal) to Sinai (Al-Hemmah, Resan Ikteifa, Himeiyir and Farsh El-Azraq) in Egypt (Fig.1). Exposures of Phanerozoic volcanic are sporadically distributed in Eastern and Western Desert, as well as the Sinai Peninsula (Fig.1).

Mid Tertiary volcanics are common in North Africa (Fig.2). They occur in the Gabal Oweinat-Arknu complex, Gabal Hassawnah, Gabal Al-Sawda, and Gabal Al-Haruj Al-Aswad in Libya, Algeria, Tunisia, and Morocco. They include the Canary Islands in the Central Atlantic offshore Northwest Africa (Fig.2). Volcanic rocks are reported in Egypt also from Kom Ombo, Gulf of Suez, Bahariya Oasis, West-Central Sinai, Wadi Araba, Gabal Qatrani north of Fayium and Gabal Khesheb west of Cairo.

The Sinai Peninsula comprises parts of the Pan-African Precambrian basement complex in the southern part and a Phanerozoic sedimentary cover that occupies the central and northern parts of Sinai. The northern part is characterized by the presence of several elongated-folds of right-en-echelon pattern, "Syrian Arc Fold System", that trend NE to ESE directions (**Krenkel, 1924**). The Syrian Arc Fold System is closely related to compressional stresses between the Afro-Arabian and Eurasian land masses when the Tethyan Sea began to close as a result of northerly subduction in the Late Cretaceous (Senonian) period (**Moustafa and Khalil, 1990**; **Jenkins, 1990**; **Abdel Aal et al., 1992**). A recent

model proposed by **Moustafa and Khalil (1995)** for deformation of northern Sinai in which they assume that the Late Cretaceous-Early Tertiary rejuvenation of the early Mesozoic passive continental margin of the Neotethys proceeded via right-lateral wrenching in northern Sinai. This model is related to the oblique convergence between Africa-Arabia and Eurasian during the closure of the Neotethys.

The Phanerozoic volcanic activities that occurred in the Lower Carboniferous to Oligo-Miocene times extruded the Precambrian basement and the sedimentary cover of Sinai in the form of dykes, sills, plugs as well as flows (**Steinitz et al., 1978**; **Musa, 1987**; **Baldridge et al., 1991**; **Ibrahim et al., 2000**; **El-Sayed, 2012**). The Oligo-Miocene volcanic activity occurs mainly as basaltic dykes trending NNW-SSE parallel to the long axis of the Red Sea and contemporaneous with the initial phase of Sinai uplifting and rifting of the Red Sea and Gulf of Suez (20-25 Ma; **Steinitz et al., 1978**). **Moon and Sadek (1921)** described these volcanics as laccoliths, interbedded with the sedimentary rocks, composed mainly of coarse-grained dolerite and exhibit onion like weathering, whereas some vein as of calcite and zeolites are also abundant. They have definite Post-Cretaceous age according to **Moon and Sadek (1921)** and **Farag and Shata (1954)**. There are dextrally offset, E-W and NE-SW faults often widely developed along the folded belt of Syrian Arc System (**Steinitz et al., 1978**). The Gabal Ikteifa dyke is such a dyke, being dextrally displaced 2.2 a K/Ar km by Mensharih fault. It postulates a K/Ar age dated 20 and 20.5 Ma± 7 Burdigalian age (**Steinitz et al., 1978**).

There are two types of igneous activity; the first phase in the mid to late Cretaceous that are an earlier and more extensive episode produced the Wadi Natash alkaline basalts and numerous small trachytic intrusions, where this phase is related to regional uplifting. The second phase of activity during Oligo – Miocene time representing by small tholeiitic basalts flows on the Red Sea Coast and along the Nile Valley, where this phase is associated with widening of the rift valley (**Ressetar et al., 1981**).

The Tertiary volcanics in north Sinai are occasionally classified petrographically into analcite-bearing basalts, alkaline olivine basalts, doleritic basalts and amygdaloidal basalts (**Abu El-Leil, 1988**). Chemically they show markedly undersaturated nature with normative nepheline and strongly sodic suite ($Na_2O/K_2O>1$). They have small Mg value and enriched in Fe and Ti, as well as relatively low content in V, Zr and Sr. According to **Zanettin (1984)** classification, by using TAS diagram they are mainly basanites and alkaline basalts, however by using the compiled diagram constructed by **MacDonald and Katsura (1964)**, **Saggerson and Williams (1964)**,

and **Irvine and Baragar (1971)**, they exhibit mildly alkaline affinity. Moreover they are coinciding with the composition of hyper-alkaline suite of Ross Island Antarctica and Hawaiian alkaline suite. Tectonically they had been formed olivine basaltic magma, with limited partial melting from mantle peridotite which developed within plate of continental environment.

The present paper will be study the field relations, petrography and geochemistry of basaltic rocks in Al-Hemmah-Resan Ikteifa district North Sinai, Egypt (Figs.3 & 4). Thirty representative bulk basaltic samples were selected from Al-Hemmah-Resan Ikteifa district. These samples were examined by using a petrographic microscope to evaluate sample texture, degree of alteration and the presence of volcanic glass in matrix.

2. Geological setting

The studied basaltic rocks occur as sheets capping the hills as well as minor sills intruding the Tertiary sediments (Figs.5 & 6a). Vertical columnar jointing is observed. The basaltic rocks appear to be dark grey to black, hard, massive and generally fresh; sometimes they are pale grey and friable at the surface, due to weathering.

The basalt extrusions traverse the chalk at Gabal Ikteifa and near Wadi Um Mitla, the latter gets harder and resists denudation and in consequence give rise to little hills **(Hume, 1962)**. Pockets of magnesium sulphate were observed in the chalk near the intrusion of Wadi Um Mitla and their origin was considered as being due to the action of the basaltic dyke there.

The Resan Ikteifa exposure is a major NE-SW-oriented asymmetric anticline in the Syrian Arc Fold System. It has a gentle northwester flank dipping at about 4-10° and a steeper southeaster flank that generally dips at about 30° and locally reaches a dip angle of about 50° (**Moustafa and Khalil, 1995**). The sedimentary rocks of Resan Ikteifa are composed of sedimentary successions related to Upper Cretaceous – Eocene age (Fig.5; **Geological Survey of Egypt, 1992** and **Omran, 1997**).

The Resan Ikteifa basaltic exposures are usually tabular and have an average thickness of about 11m; except for the exposure 1.2km south of Al-Hemmah Village which is only 5m thick, and seems to have been subjected to the extensive weathering and erosion. The basaltic sheets and the underlying sediments dip at angles varying between 30° and 50° as noticed in the Resan Ikteifa exposure (Fig.6b).

Al-Hemmah basalt occurring in form flow hills, dykes, and plugs as topographic feature with different in shape and thickness. This black color when fresh, but is usually decomposed on the surface to soft green rock falling to pieces at the least touch related to Tertiary volcanic basalt. Two basaltic exposures crop out at Al-Hemmah in an E-W and NE-SW trends

along a distance of 3km and 1km respectively. It seems probable that they are localized along a fault forming a fault scarp. The underlying rocks of the Al-Hemmah basaltic flows are related to the Thebes (Upper Libyan) and Sudr (Maastrichtian) formations.

The volcanic extrusions developed contact metamorphic aureoles in the adjacent sedimentary rocks, which are winder in the northern part than in the central and southern parts of Sinai Peninsula. These aureoles were mapped as metamorphosed limestone by the **Geological Survey of Egypt (1992)** in northern Sinai.

1.Bahariya
2.Gabal Qatrani
3.Abu Roash
4.Abu Treifiya
5.Abu Zaabal
6.El-Bahnasa
7.Tahna
8.El-Quseir
9.Gabal Abu Zurub
10.Rageibet el Naama
11.Gabal Hammam Faraun
12.Al-Hemmah
13.Gabal Ikteifa
14.Gabal Hassana
15.Gabal Mensharih
16.Wadi Mehashim

17.Wadi Budra
18.Farsh El-Azraq
19.Gabal Uweinat and Bir Safsaf
20.Wadi Araba- Abu El-Darag area
21.Wadi Natash volcanic field
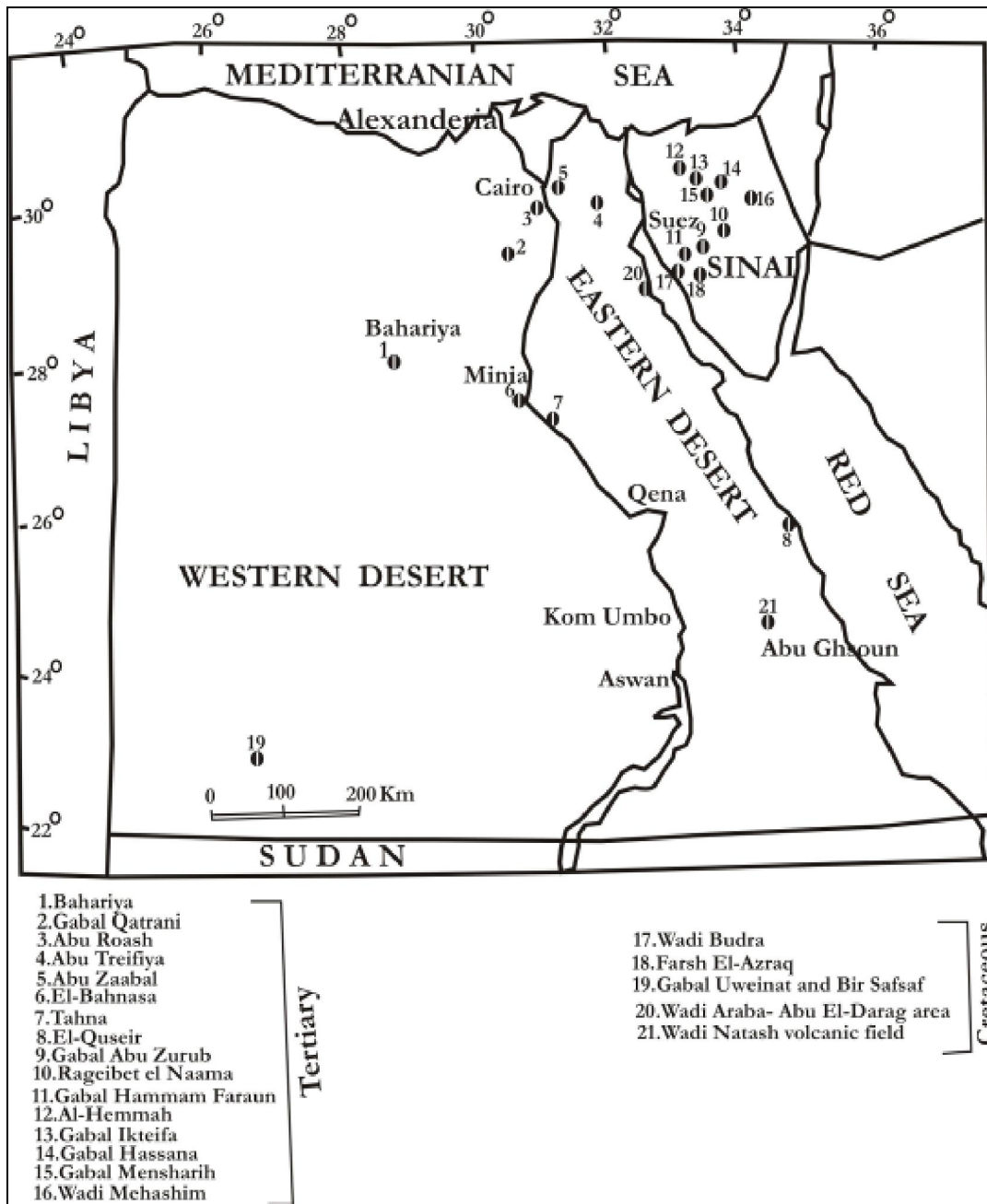
Tertiary

Cretaceous

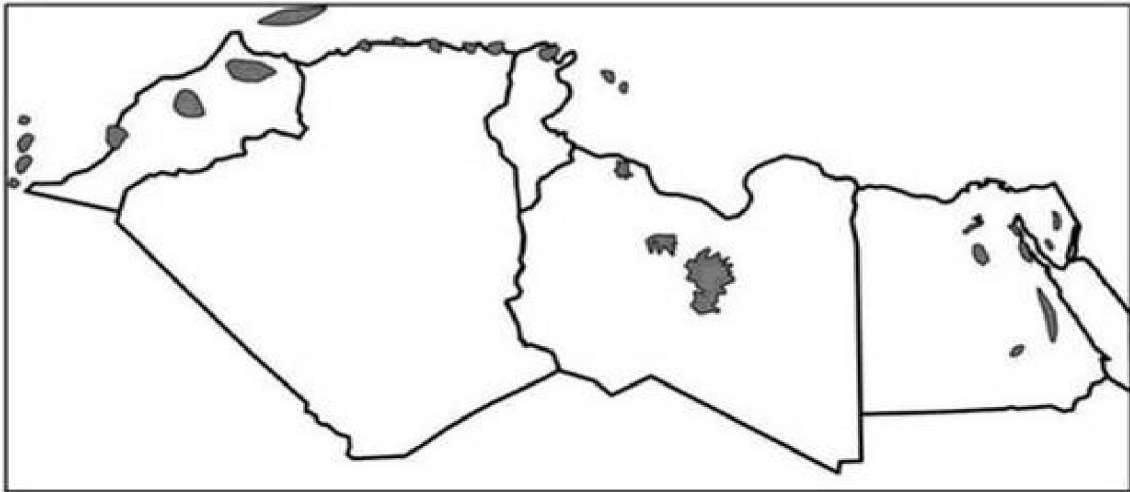Fig.1. Distribution map of some basaltic occurrences in Egypt.

Fig.2. Cenozoic igneous volcanics in North Africa (**Tawadros, 2001; Lustrino and Wilson, 2007**).
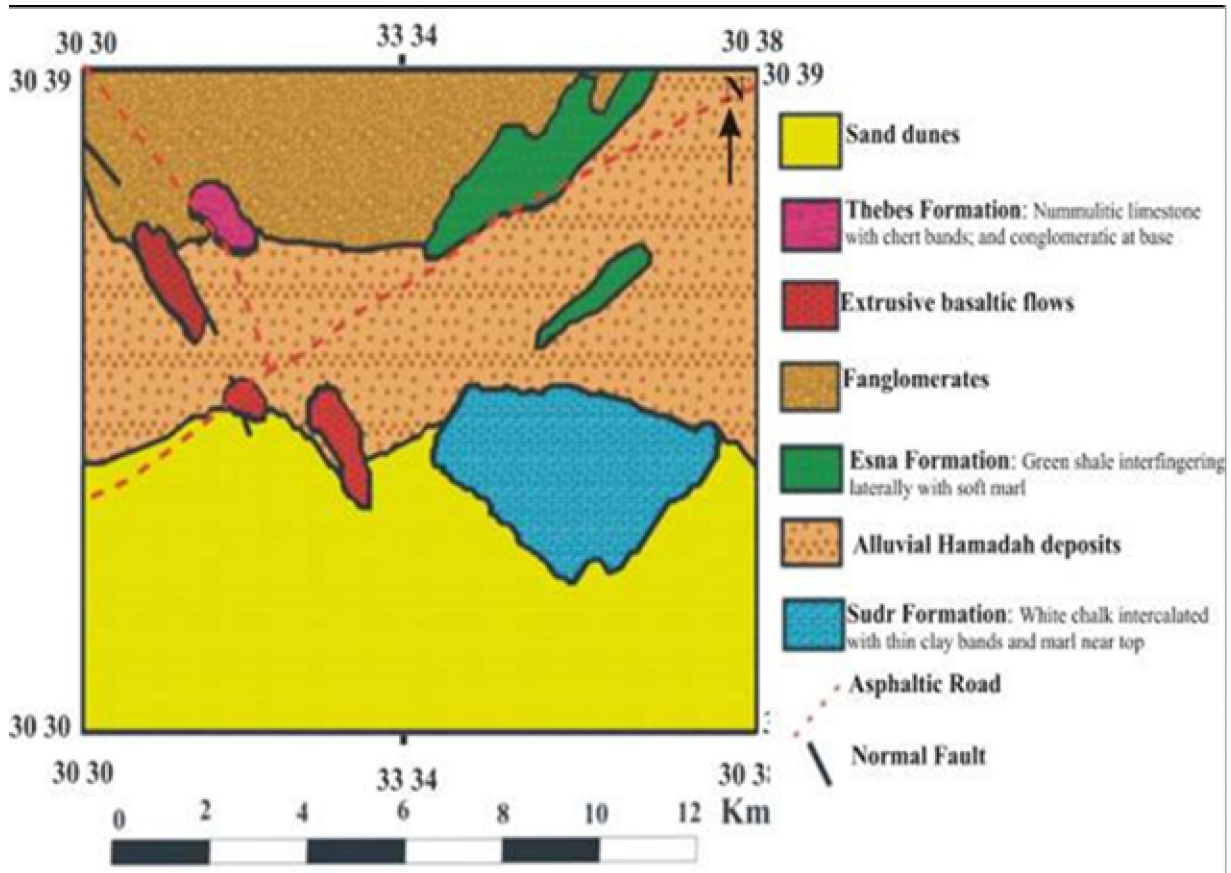

Fig.3. Geological map of the Al-Hemmah area, North Sinai, Egypt (**EGPS, 1993a**).
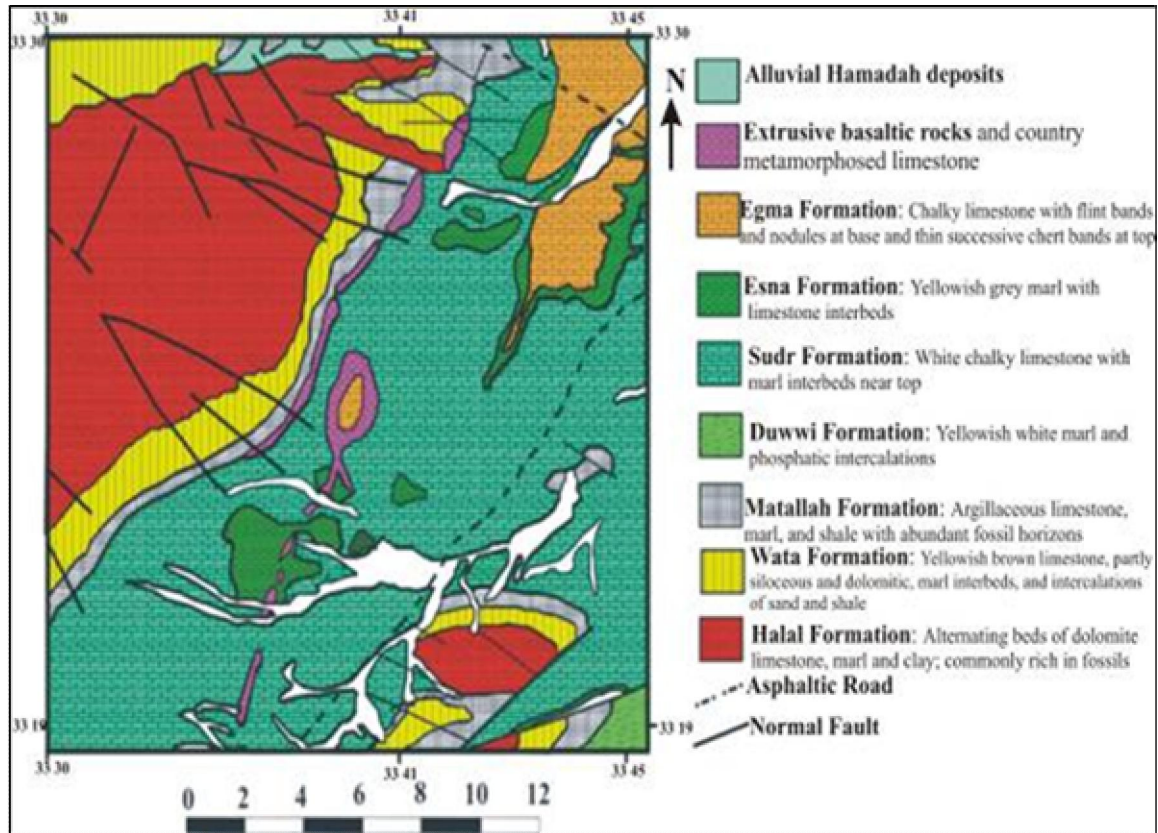
Fig.4. Geological map of the Resan Ikteifa area east Gabal Yelleq, North Sinai, Egypt (**EGPS, 1993b**).

The Tertiary basaltic dykes and sills of Resan Ikteifa east of Gabal Yelleq and extending northward to Gabal Al-Maghara extruded the sedimentary rocks with a curved attitude in the map given by **Baldridge et al. (1991)**. The studied Tertiary basaltic dykes and sills trend is NE-SW and NW-SE in the southern and northern parts, respectively.

The contact metamorphism observed in the rock underlying these basalts and not in the overlying sediments, the presence of a vesicular layer in the exposure just south of Al-Hemmah Village, and the marked weathering of the upper surface in each exposure indicate that these basaltic bodies were lava flows and not extrusive sheets.

The underlying rocks of the Resan Ikteifa basaltic sheets are related mainly to the Matallah Formation (Santonian-Coniacian; Fig.6c), which composed of chalky limestone with yellowish grey marl intercalation at its top (**Omran, 1997** and **Issawi et al., 1999**). The Resan Ikteifa basaltic sheets also extruded within Thebes (Upper Libyan) and Sudr (Maastrichtian) formations. Thebes Formation consists of white thin-bedded limestone with chert bands and Nummulite fossils in parts (Fig.6d) and Sudr Formation consists of white chalky limestone with marl interbeds near top. The volcanic sill created a contact metamorphic aureole of varying width the

rocks show varies colors along the contacts. The dolerite still sends sometimes tongue-like (apophyses) into the adjacent metamorphosed limestone (**Abu El-Enen, 2001**).

The contact between the extrusive basaltic rocks of the Al-Hemmah and Resan Ikteifa volcanism is also marked by the presence of contaminated country dark grey rocks (Figs.6b & 6d) and metamorphosed limestone, related to the basaltic extrusion. While no contact metamorphism is observed in some localities of Resan Ikteifa, the thermal effect of the lava flows is clear on the underlying chalky and thin-bedded limestones which changes to compacted massive dark grey limestone. The limestone is hard and crystalline with a dark grey weathered color.

3. Petrography

The studied basaltic rocks in the Al-Hemmah-Resan Ikteifa district could be classified microscopically into: 1) Olivine dolerites at Al-Hemmah area. 2) Porphyritic olivine basalts at Resan Ikteifa area. Al-Hemmah and Resan Ikteifa volcanic rocks are almost identical, being formed mainly of non-porphyritic olivine dolerite together with some porphyritic olivine basalts. The following is a brief description of the mineralogical composition of the studied basalts.
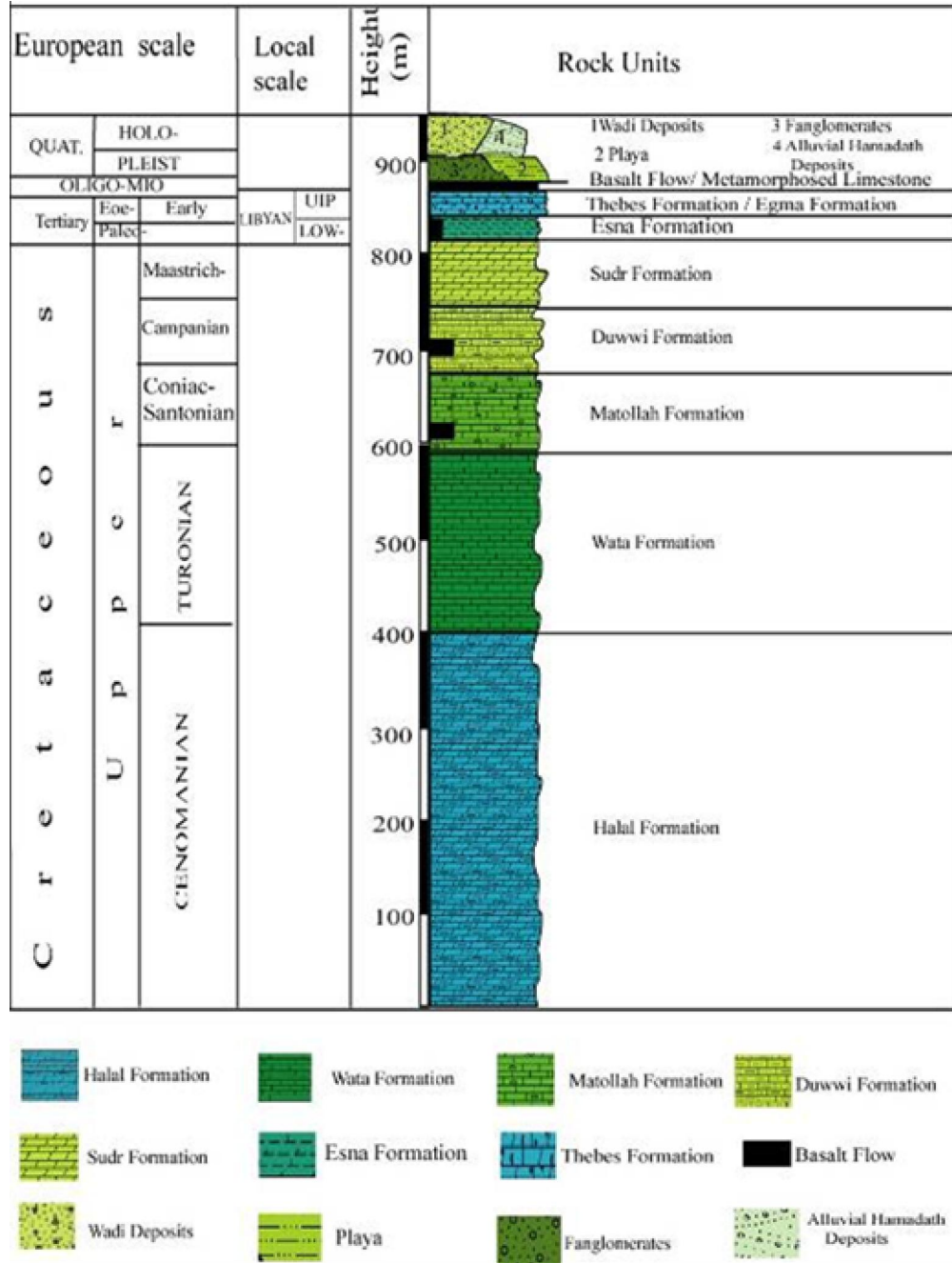
Fig.5. Lithostratigraphic section of Al-Hemmah – Resan Ikteifa district, North Sinai, Egypt.

3.1. Olivine dolerites

The chief mineralogical constituents are plagioclase (An_{46}-An_{55}), clinopyroxene (augite and titanaugite), as well as olivine. Minor constituents are opaque minerals with subordinate amounts of apatite. Secondary minerals are few and include iddingsite, serpentine, and chlorite. Nepheline is present in small amounts in many these dolerites. They are usually holocrystalline, medium-grained rocks that show ophitic and subophitic textures.

Plagioclase (Pl) occurs as euhedral to subhedral prismatic crystals and more or less uniform in size although they occur as large phenocrysts. Some plagioclase crystals exhibit Carlsbad and percline twinning and frequently exhibit diffuse zoning (Fig.7a). Few plagioclase crystals are slightly saussuritized. The plagioclase crystals form doleritic and subdoleritic textures (Fig.7b), depending on whether the intergranular spaces between them are filled with single crystals of olivine and pyroxene, or aggregates of both, respectively.
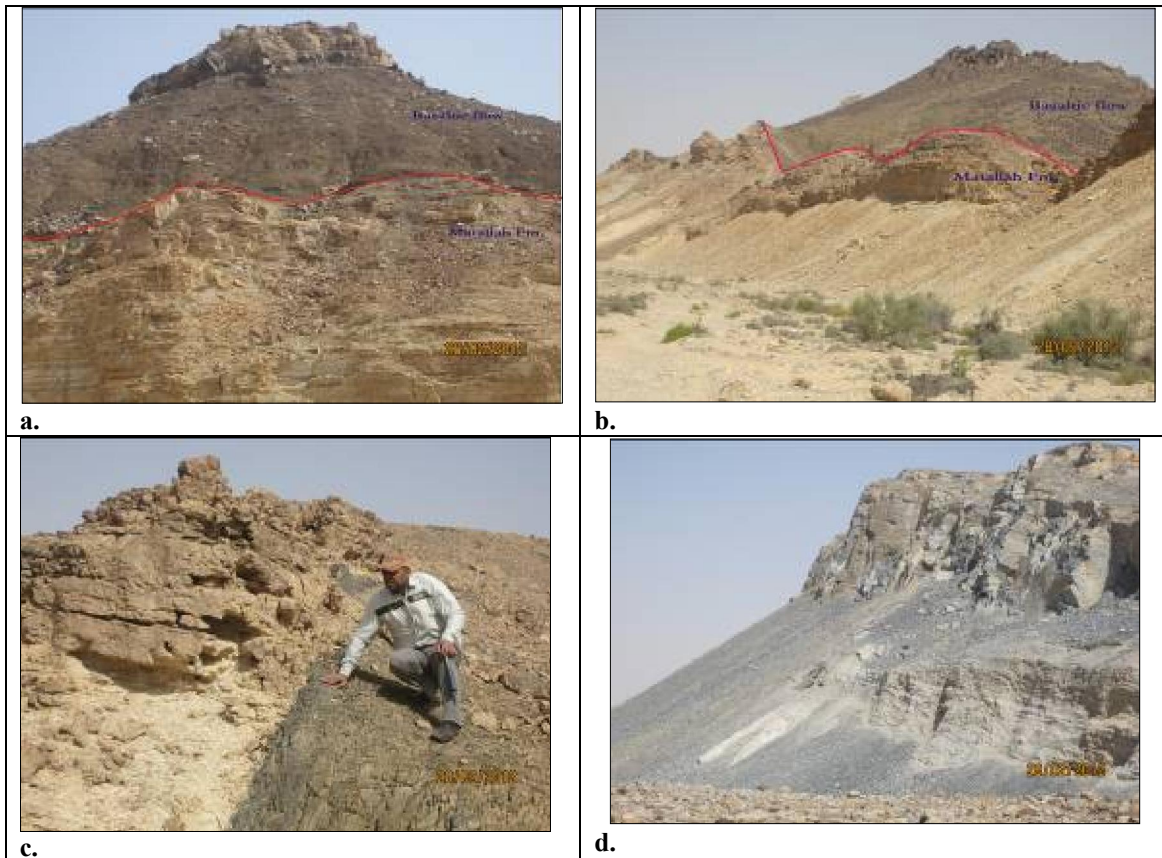
Fig.6 (a-d). Field photographs showing some rock units at the studied district.
a. Resan Ikteifa basaltic sheet overlying white thin-bedded limestone of Matallah Formation (Looking NE).
b. Basaltic sheets and the underlying sediments of Matallah Formation dip at angles varying between 30° and 50° as noticed in the Resan Ikteifa exposure (Looking NW).
c. Sharp contact between Resan Ikteifa basaltic rocks and chalky limestone of Matallah Formation (Looking NE).
d. Contaminated dark grey rocks (Hybrid zone) underlying the Resan Ikteifa basaltic exposures and overlying white thin-bedded limestone of Thebes Formation.

Some plagioclase phenocrysts enclose opaque minerals parallel to, and partly obscuring the lamellar twinning.

Augite clinopyroxenes are generally pale brown color, but a more intense purplish-brown color is also observed in some samples. The maximum extinction angle is about 45, which indicates an augitic composition. Titanaugite is also identified with brownish green color. They vary in size from 1.3mm to 1.9mm and finer-grained crystals from 0.3mm to 0.7mm in length. Pyroxenes ophitically enclose small crystals of plagioclase (Fig.7c); while the finer-grained aggregates are arranged in subophitic and glomeroporphyritic textures.

Olivine (ol) is usually developed as small anhedral rounded granules either enclosed in pyroxenes or aggregated with the intergranular spaces

between plagioclase laths with an average diameter of about 0.4mm. It is apparently of early crystallization, being sometimes poikilitically enclosed within subhedral pyroxene phenocrysts forming a cumulate texture. The crystals enclosed in pyroxene are usually serpentinized along borders and cracks; advanced stages of alteration are shown by pseudomorph of olivine by green chlorite and finally by reddish brown iddingsite (id, Fig.7d).

Opaque minerals (op) are relatively abundant and are frequently penetrated by crystals of silicate minerals. They occur as granules and as small subhedral to euhedral crystals, which are occasionally skeletal (Fig.7a). They are represented by titanomagnetite and ilmenite. They also occur as disseminated crystals or present as euhedral cubes like

crystals probably after ferrugination process. They occur as accessory minerals in these rocks.

3.2. Porphyritic olivine basalts

Porphyritic olivine basalts are fine- to medium-grained and consist essentially of plagioclase, olivine, and titanaugite (tau) phenocrysts. Opaque minerals occur as accessory minerals.

Meanwhile saussurite, epidote and calcite are secondary minerals occurs as alteration products. They are plagioclase- and pyroxene-phyric basalts with a fine-grained groundmass. The groundmass is composed mainly of plagioclase and opaque minerals with lesser amounts of clinopyroxene and olivine. Glass is also present. Porphyritic texture is one of the most characteristic textures in this basalt. Glomeroporphyritic, hyalopelitic and pilotaxitic textures are common.

Plagioclase is usually the principal mineral found in the rock and occurs either as phenocrysts (Fig.8a) or as a major groundmass constituents the plagioclase phenocrysts occurs as euhedral to subhedral prismatic, lath-shaped, randomly oriented, inequdimentional crystals. Some plagioclase phenocrysts reaching up to 1.3mm in length are embedded in a fine-grained groundmass of plagioclase, opaque minerals and pyroxene. Few plagioclase phenocrysts poikilitically enclose fine, randomly scattered granules of opaque minerals and pyroxenes (Fig.8b & c). They are partially altered to saussurite, epidote and calcite. Plagioclase sometimes occurs in normally zoned crystals, Carlsbad and percline twinning. Both porphyritic and glomeroporphyritic textures are recorded in addition to subophitic texture (Fig.8b & c).

The olivine forms 10-15% by volume of the basalt. It forms small, rounded crystals either embedded in the groundmass (Fig.8b) or enclosed poikilitically within the pyroxene phenocrysts. It is partially altered along borders and cracks to reddish-brown iddingsite and in some cases is completely altered.

Pyroxene (px) forms 20-55% by volume of the basalt and occurs as phenocrysts and granules. It is mainly composed of titanaugite of brownish green color which form large subhedral crystals of irregular boundaries enclosing sometimes randomly oriented laths of plagioclase forming subophitic texture (Fig.8b & c). The pyroxene reaches about 0.8mm in length and 0.3mm in width.

Opaque minerals form reddish brown irregular particles dispersed in the interstitial spaces between the other mineral constituents (Fig.8b & c). They are sometimes exhibit fine-grained penetrative the groundmass. The opaque minerals in the groundmass range from 0.04 to 0.07mm in diameter and are distributed more or less evenly throughout the rock,

while microphenocrysts range from 0.14 to 0.34mm in length. Glass is an important constituent in the basalt. It mostly occupies irregular to acicular areas or patches of isotropic glass (Fig.8d).

4. Analytical techniques

Out of the 30 samples collected from the Al-Hemmah – Resan Ikteifa district basaltic rocks, 11 were selected for whole rock major oxides, and trace element analyses. All analyses were done at the Central Laboratory in Nuclear Materials Authority (NMA), Egypt.

XRF (Model: Thermo-JarretAsh ENVIRO II) was used to analyze major elements, whereas ICPMS (Model: Perkin Elmer Sciex ELAN 6000) was used to determine trace element concentrations. The precision is approximately 5 and 5–10% for the major oxides and trace elements, respectively, when reported at $100 \times$ detection limit.

5. Geochemistry

Chemical analyses for major oxides and trace elements of the studied basalt samples are given in Tables (1 & 2). The average of these analyses are compared with other basalts from published data by **Wilson (1989**; Table 5). The dominantly basalt-associated elements, namely combined silica (as silicate), SiO_2, Al_2O_3, CaO, Na_2O, TiO_2, K_2O, Fe_2O_3 and MgO, are higher in the Al-Hemmah and Resan Ikteifa basaltic rocks.

5.1. Major oxides and trace elements

From the obtained results, the following characteristics of the studied basalts can be given:-

They possess silica contents ranges from 45.5% to 48% with an average 46.56% are silica saturated. It is clear that the increase in SiO_2 is accompanied by decrease in TiO_2, K_2O, P_2O_5 and LOI. Al_2O_3 ranges from 12.3% to 14.5 % with an average 13.48%. The studied basaltic rocks possess high concentrations of Fe_2O_3+FeO (11.4 to 13.5%), CaO (8 to 10.7%), MgO (5.5 to 8%), TiO_2 (2.6 to 3.8%), Na_2O (2.1 to 3.1%), K_2O (1 to 1.5%), P_2O_5 (0.46 to 0.72%), and MnO (0.13 to 0.27%).

The high concentration of MgO and Fe_2O_3+FeO coupled with low concentrations of TiO_2 and K_2O also point to a depleted upper mantle earlier eruptions which extracted magmas of basaltic compositions which was rendered refractory by **Mysen and Kushiro 1977**). The behavior of MgO in Al-Hemmah basalt is unusual being increased with magmatic evolution. Sodium displays trends of slight diminishing with SiO_2 increasing in Al-Hemmah volcanites, while in Resan Ikteifa the contents of Na increase.

The high concentrations of Ni, Co, and Cr especially in these basalts accentuate the notion for the depletion of the upper mantle. The concentrations

of alkalis in these basalts could have been due to normal magmatic fractional crystallization processes.

Variations of trace elements are shown on figures (10, 11 & 12). The two studied volcanites display similar trends for Cr, Ni, V, Rb having decreasing contents with magmatic evolution. For Ba the opposite trend is manifested. Other elements do not display clear trends.

They are characterized by high concentrations of the incompatible trace elements Ba, Sr, V, Zn, Cr and Zr. The enhancement in the concentrations of potassium and incompatible trace elements suggests enrichment of these elements in the upper mantle before eruption. These rocks exhibit low concentrations of P_2O_5, MnO, Ni, Cu, Rb, Y, Pb, Ga, and Nb contents.

The studied basalts display average in MgO (6.72%) that is essentially the same as mid-ocean ridge basalts (MORB) and alkali olivine basalts (hawaiites) of the Hawaiian Islands, with high Na_2O and TiO_2 compared to MORB and classical tholeiitic fractionation trends on MgO variation diagrams (Figs.9 & 10). The flat FeO*, SiO_2 and Al_2O_3 trends and the increase in titanium with decreasing MgO, all imply that olivine is the dominant fractionating phase. The coupling of higher silica with high alkalis is unusual and distinguishes the basalts from normal alkali basalts, which typically have lower silica contents.

Trace element concentrations for studied basalts are equally distinct. Compared to the tholeiitic basalts, the high-Na alkaline basalts (hawaiites) are higher in Zn, Sr, Zr, V and lower in Rb, Y, Cu (Figs.11 & 12).

The chemical composition of the studied basalts quite coincides with the chemical composition of hyperalkaline suite of Rose Island and Antractica (H.S) and Hawaiian alkaline suite (H.A.S; Fig.13; **Middlemost, 1985**).
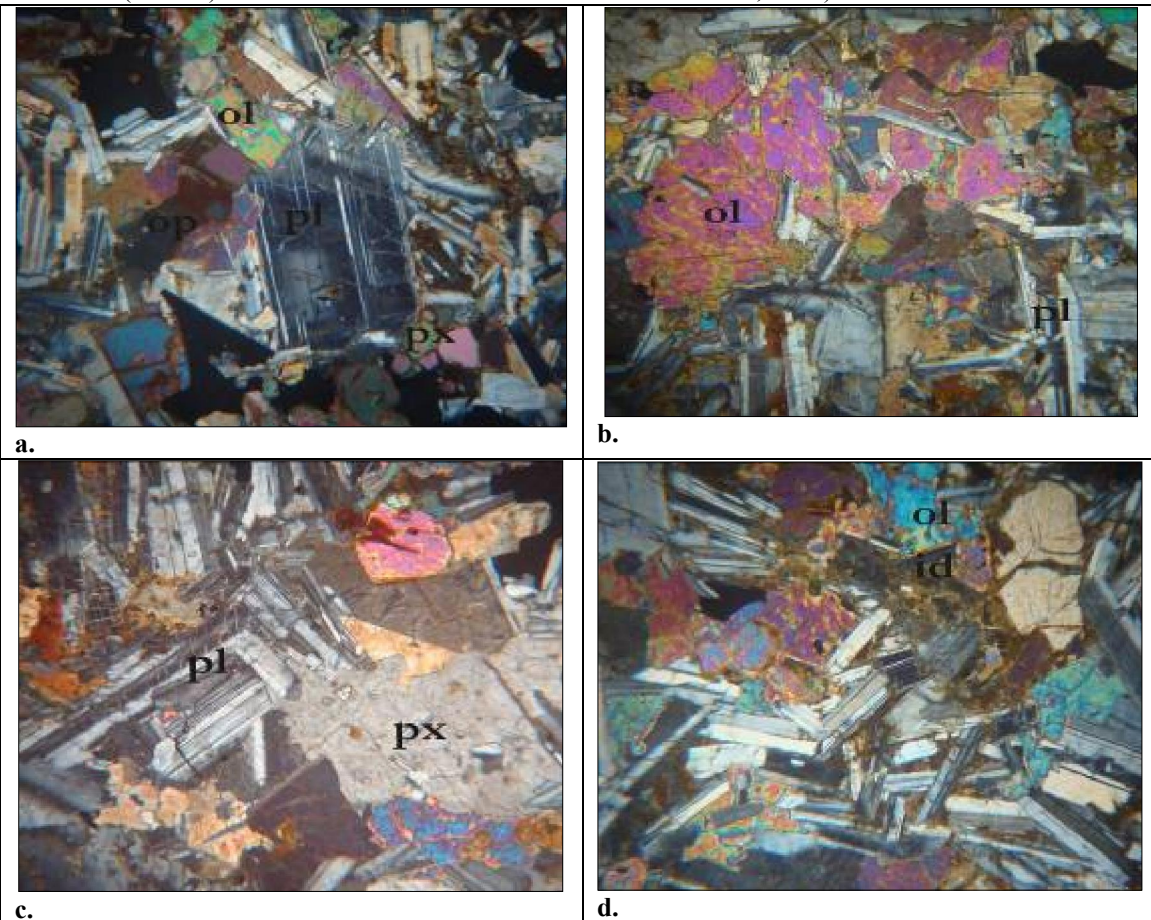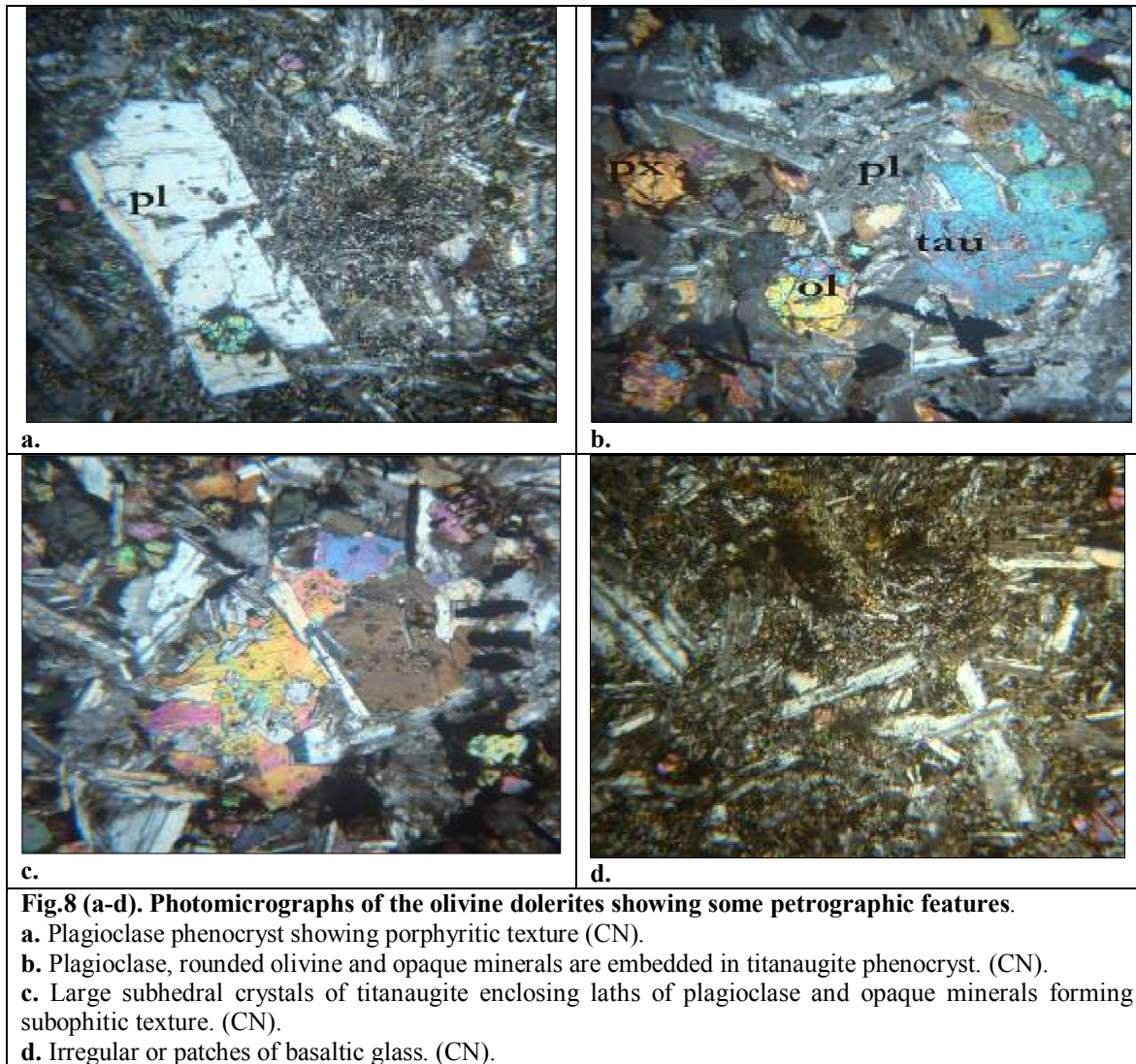

Fig.7 (a-d). Photomicrographs of the olivine dolerites showing some petrographic features.
a. Zoned plagioclase and opaque minerals. (CN).
b. Doleritic and subdoleritic textures. (CN).
c. Pyroxenes ophitically enclose small crystals of plagioclase. (CN).
d. Alteration of olivine by reddish brown iddingsite along borders and cracks. (CN).

Fig.8 (a-d). Photomicrographs of the olivine dolerites showing some petrographic features.
a. Plagioclase phenocryst showing porphyritic texture (CN).
b. Plagioclase, rounded olivine and opaque minerals are embedded in titanaugite phenocryst. (CN).
c. Large subhedral crystals of titanaugite enclosing laths of plagioclase and opaque minerals forming subophitic texture. (CN).
d. Irregular or patches of basaltic glass. (CN).

5.2. Geochemical classification

The studied basaltic rocks of Al-Hemmah-Resan Ikteifa district contain significant normative hypersthene (*hy*) instead of nepheline (*ne*), usually accompanied by olivine (*ol*; Table 4). The chemical classifications of these rocks are olivine tholeiites, according to **Williams *et al.* (1985)** who classified the major basaltic rock types, in order of increasing under saturation in SiO_2, will be named as follows:
1. Tholeiites:
a. Slightly over saturated; normative *Q* and abundant *hy*.
b. Saturated; abundant normative *hy*.
2. Olivine tholeiites: under saturated; normative *ol* and *hy*.
3. Olivine basalts: under saturated; normative *ol*; *hy* insignificant or completely lacking.

4. Alkali olivine basalts: Strongly under saturated; normative *ol* and minor *ne*.
5. Basanites: Strongly under saturated; *ol* and significant *ne* in the norm.

According to the petrography characteristics and normative mineral compositions (Table 4), the studied basalts are proved to be alkali olivine basalts (Samples 2, 3, 7 & 8), olivine basalts (Samples 1, 6, 9, 10 & 11) and olivine tholeiites (Samples 4 & 5). Nepheline as a normative compound or as a mineral is present in some of the Al-Hemmah - Resan Ikteifa volcanics.

The petrographic classification of the basaltic rocks was confirmed chemically by plotting the analytical data on the Na_2O+K_2O versus SiO_2 binary diagram of **Cox *et al.* (1979)**. On this diagram (Fig.14a), all the data plot within the fields of alkali olivine basalts and tholeiitic basalts.

The classification of the studied basaltic rocks carried out by using the log (Nb/Y) versus log $(Zr+Ti_2O)*0.0001$ binary diagram (Fig.14b) of **Winchester and Floyd (1977)**. On this diagram all the studied basaltic rocks plot in the alkaline basalts.

The classification scheme based on the proportion of their calculation percentage Fe$_2$O$_3$+FeO+MgO, Al$_2$O$_3$ and MgO (**Rickwood, 1989**) was applied. On the diagram, whole of the studied basalts fall in the field high-Fe tholeiitic basalts (Fig.14c). On the total alkali silica (TAS) diagram (Fig.14d) of **Le Maître (2002)**, the plotted basaltic samples fall in the field of basalts.

5.3. Alteration and mobility of elements

Schweitzer and Kröner (1985) used the CaO/Al$_2$O$_3$-MgO/10-SiO$_2$/100 ternary diagram to display the mobility of elements in basalts. The analyzed samples plot inside the field of fresh volcanic rocks (not altered basalt, Fig.15a).

On the (Na_2O+K_2O) versus $\{K_2O/(Na_2O+K_2O)\}*100$ variation diagram (Fig.15b) of **Hughes (1973)** showing the studied basaltic samples plot in the field of unaltered igneous rocks.

Al-Malabeh (1993) used the $K_2O/(Na_2O+K_2O)$ versus TiO_2/P_2O_5 binary diagram of **Chandrasekharam and Parathasarathy (1978)** to discriminate between rift volcanics of crustal fragmentation and plateau volcanic of true continental origin. It is clear that the studied basaltic samples are plateau volcanic of true continental origin (Fig.15c).

Table 1. Major oxide contents (wt %) of the Al-Hemmah and Resan Ikteifa basaltic rocks.

Oxides	Al-Hemmah						Resan Ikteifa					Mean
	1	2	3	4	5	6	7	8	9	10	11	
SiO$_2$	46.5	45.7	45.2	47.3	48	47.5	46.5	45.5	47	46.5	46.5	46.56
Al$_2$O$_3$	14.5	13.6	14	13.5	12.5	12.3	12.5	13.7	14	13.7	14	13.48
Fe$_2$O$_3$*	13.5	12.3	11.9	13	12	11.4	11.7	12	11.5	12.5	12	12.16
CaO	9	10	9.8	9.5	10.2	10.3	10.7	10	9.5	9	8	9.64
MgO	5.5	7	8	7.1	7.4	6.8	7	7	6	5.9	6.2	6.72
K$_2$O	1.4	1.2	0.9	1	0.8	1.3	0.9	1	1.5	1.1	1.3	1.13
Na$_2$O	2.5	3	2.8	1.9	2.1	2.7	3.1	2.8	2.5	3.2	3	2.69
MnO	0.13	0.14	0.2	0.21	0.23	0.19	0.18	0.27	0.16	0.15	0.21	0.19
TiO$_2$	3.2	2.8	2.4	3	2.6	2.7	3	3.2	3.5	3.8	3.1	3.03
P$_2$O$_5$	0.53	0.72	0.63	0.5	0.57	0.54	0.7	0.6	0.5	0.46	0.72	0.59
LOI	3.2	3.7	3.4	3	3.2	3.1	3.2	3	3.3	3.4	4	3.32
Total	99.96	100.1	99.23	100.1	99.6	99.1	99.3	99.1	99.5	99.7	99.2	99.54
Ti	1.92	1.68	1.44	1.80	1.56	1.62	1.80	1.92	2.10	2.28	1.86	1.82
Mg#	0.29	0.36	0.40	0.35	0.38	0.37	0.37	0.37	0.34	0.32	0.34	0.35

5.4. Magma type

Gass (1970) reported that the tertiary basaltic magma within Afro-Arabian dome is due to crustal deformation to include:-

1. Alkali basalts concurrent with vertical uplift of the dome.

2. Transalkaline basalts (lava intermediate in composition between alkali basalts and tholeiite and that characteristically produce peralkaline rhyolite on fractionation) in zone of crustal attenuation.

3. Tholeiitic basalts in area of new oceanic crust.

Abdel Meguid (1992) and **El-Desoky *et al.* (2015**) revealed that the presence of two main continental basaltic rock types: High-TiO$_2$ basalt and low- TiO$_2$ basalt based on geochemical ground of some incompatible elements. This means the presence of two independent magma types. Mean chemical composition of Al-Hemmah - Resan Ikteifa basalts are fairly comparable with high-TiO$_2$ basalt. This supports that High-TiO$_2$ magma source is responsible for the derivation of the studied Al-Hemmah - Resan Ikteifa basalts.

The alkaline character of the Al-Hemmah basalt is indicated by total alkali silica diagram. On the total alkalis versus SiO$_2$ binary diagram of **Irvine and Baragar (1971)**, most of the analyzed samples plot in the alkaline field (Fig.16a) but two samples of Al-Hemmah basaltic rocks plot within subalkaline field due to low value of alkali metals.

The AFM ternary diagram (Fig.16b) of **Irvine and Baragar (1971)** shows the studied basaltic samples originated from tholeiitic magma rich in total iron contents.

The ANK versus ACNK variation diagram (Fig.16c) places all the studies basaltic samples in the meta-aluminous field due to the moderate content Al$_2$O$_3$ on the magma type diagram of **Maniar and Piccoli (1989)**.

Table 2. Trace element contents (ppm) of the Al-Hemmah and Resan Ikteifa basaltic rocks.

Samples	1	2	3	4	5	6	7	8	9	10	11	Mean
Cr	107	110	106	135	172	160	88	80	113	77	80	111.64
Ni	60	62	57	74	79	76	40	45	66	43	45	58.82
Cu	66	70	63	66	54	59	45	50	60	68	70	61.00
Zn	132	135	130	96	101	105	104	110	109	81	75	107.09
Zr	123	127	120	113	106	110	151	145	106	130	125	123.27
Rb	29	30	27	27	23	25	49	40	21	26	28	29.55
Y	25	27	23	23	22	24	29	25	22	27	24	24.64
Ba	905	910	890	817	718	760	1053	901	885	920	950	882.64
Pb	6	7	5	10	6	9	3	4	7	7	8	6.55
Sr	734	740	715	681	639	650	909	895	640	785	795	743.91
Ga	20	21	19	15	18	17	10	9	12	13	14	15.27
V	415	420	410	415	370	390	473	460	419	426	440	421.64
Nb	27	30	25	24	23	22	33	31	23	29	31	27.09
Ti	19200	16800	14400	18000	15600	16200	18000	19200	21000	228000	18600	18200

Mg# =Mg member (MgO/MgO+Fe_2O_3+FeO)

Table 3. Some ratios of the Al-Hemmah and Resan Ikteifa basaltic rocks.

	1	2	3	4	5	6	7	8	9	10	11	Mean
Fe/Mg	2.45	1.76	1.49	1.83	1.62	1.68	1.67	1.71	1.92	2.12	1.94	1.8
Na_2O/K_2O	1.79	2.50	3.11	1.90	2.63	2.08	3.44	2.80	1.67	2.91	2.31	2.38
CaO/Al_2O_3	0.62	0.74	0.70	0.70	0.82	0.84	0.86	0.73	0.68	0.66	0.57	0.69
Zr/Nb	4.56	4.23	4.80	4.71	4.61	5.00	4.58	4.68	4.61	4.48	4.03	4.55
V/Zr	3.37	3.31	3.42	3.67	3.49	3.55	3.13	3.17	3.95	3.28	3.52	3.42
Ti/V	46.27	40.00	35.12	43.37	42.16	41.54	38.05	41.74	50.12	53.52	42.27	43.16
Nb/Y	1.08	1.11	1.09	1.04	1.05	0.92	1.14	1.24	1.05	1.07	1.29	1.1
Y/Nb	0.93	0.90	0.92	0.96	0.96	1.09	0.88	0.81	0.96	0.93	0.77	0.91

Table 4. Normative mineral composition of the Al-Hemmah and Resan Ikteifa basaltic rocks.

|	**1**	**2**	**3**	**4**	**5**	**6**	7	8	**9**	**10**	**11**
Or	8.12	6.94	5.23	5.76	4.65	7.59	5.29	5.82	8.7	6.41	7.65
An	23.83	19.79	22.81	24.67	22.07	17.78	17.36	21.75	22.38	19.53	20.79
Ab	20.8	20.72	21.17	15.73	17.59	22.57	23.39	22.66	20.97	26.72	25.28
Di	14.04	20.31	17.72	14.99	20.16	24.64	25.41	19.64	17.52	18.02	11.82
Hy	9.52	0	0	20.29	22.12	3.25	0	0	9.42	0.97	8.88
Ol	10.54	16.8	19.81	6.15	1.41	12.37	13.96	16.5	7.45	14.1	11.49
Mt	2.73	2.59	2.5	2.6	2.5	2.6	2.51	2.53	2.46	2.63	2.56
IIm	5.99	5.25	4.53	5.57	4.89	5.08	5.84	6.07	6.6	7.15	5.88
Ne	0	2.29	1.31	0	0	0	1.39	0.5	0	0	0
Ap	1.1	1.49	1.31	1.03	1.18	1.12	1.44	1.25	1.03	0.95	1.49
A/CNK	0.66	0.56	0.6	0.63	0.55	0.5	0.49	0.57	0.61	0.6	0.67
A/NK	2.58	2.18	2.51	3.2	2.89	2.11	2.06	2.41	2.44	2.12	2.21
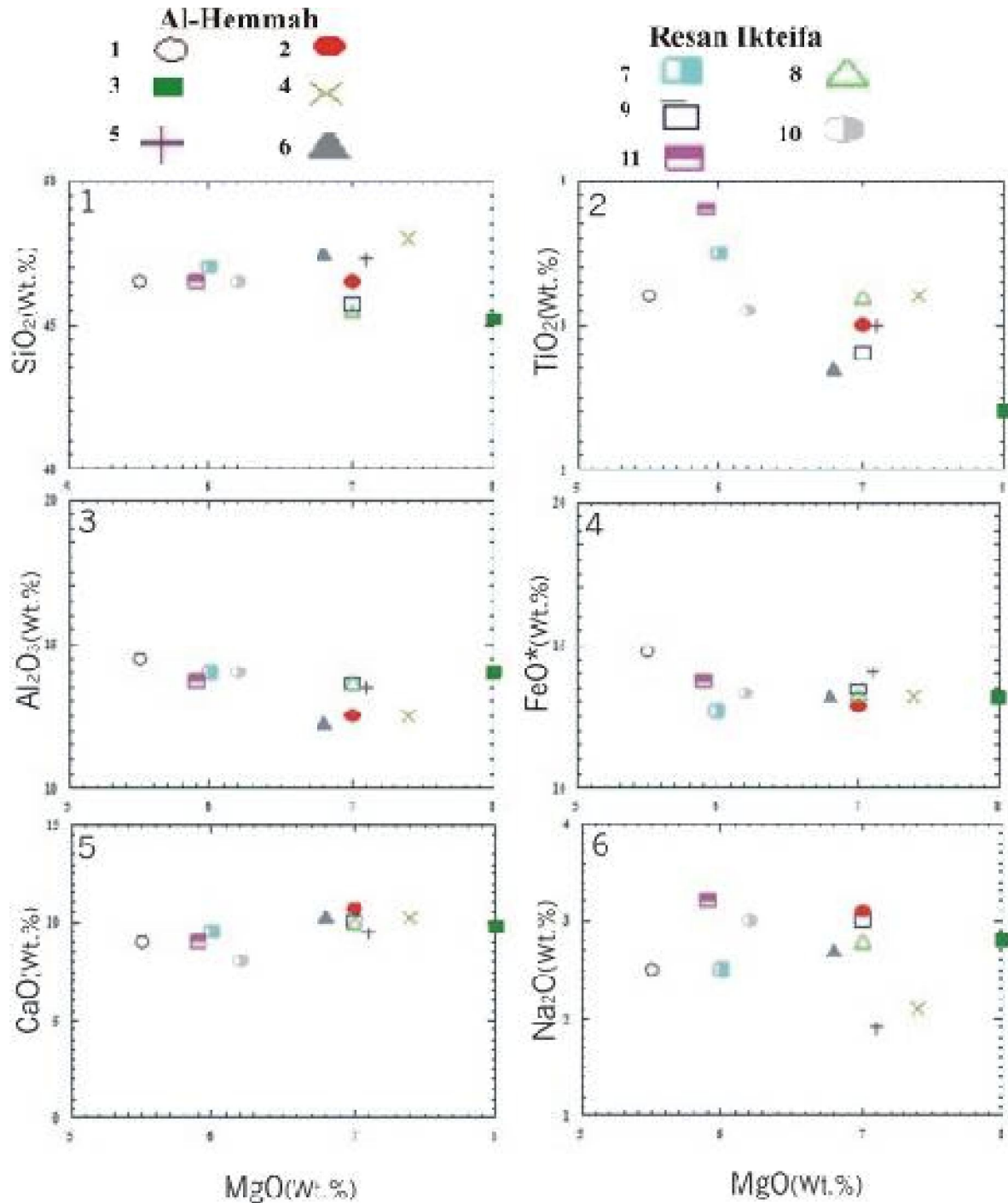
Fig.9. MgO variation diagrams of the studied basaltic samples: (1) SiO₂, (2) TiO₂, (3) Al₂O₃, (4) FeO*, (5) CaO, (6) Na₂O.
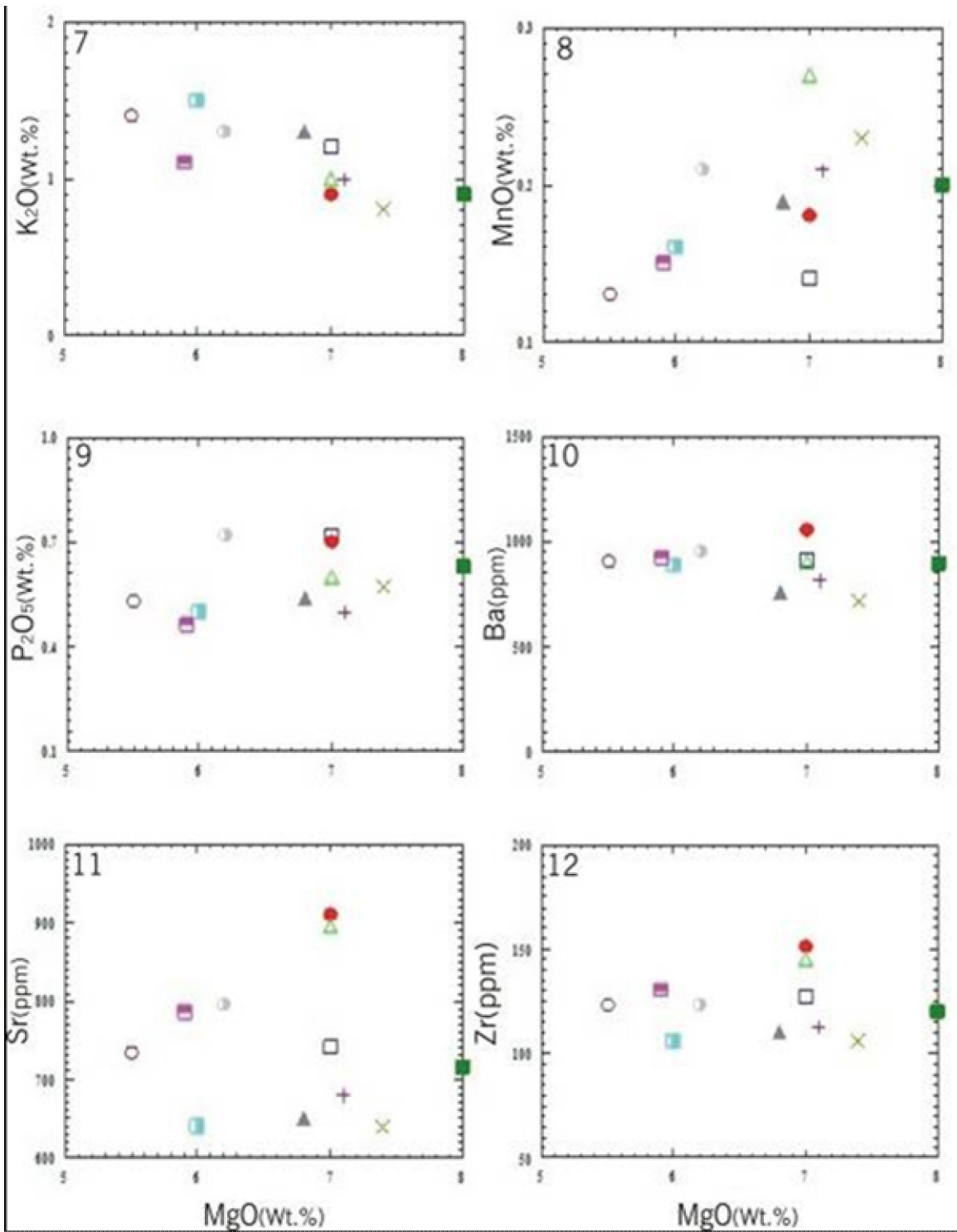
Fig.10. MgO variation diagrams of the studied basaltic samples: (7) K₂O, (8) MnO, (9) P₂O₅, (10) Ba, (11) Sr, (12) Zr. Symbols as in Figure (9).
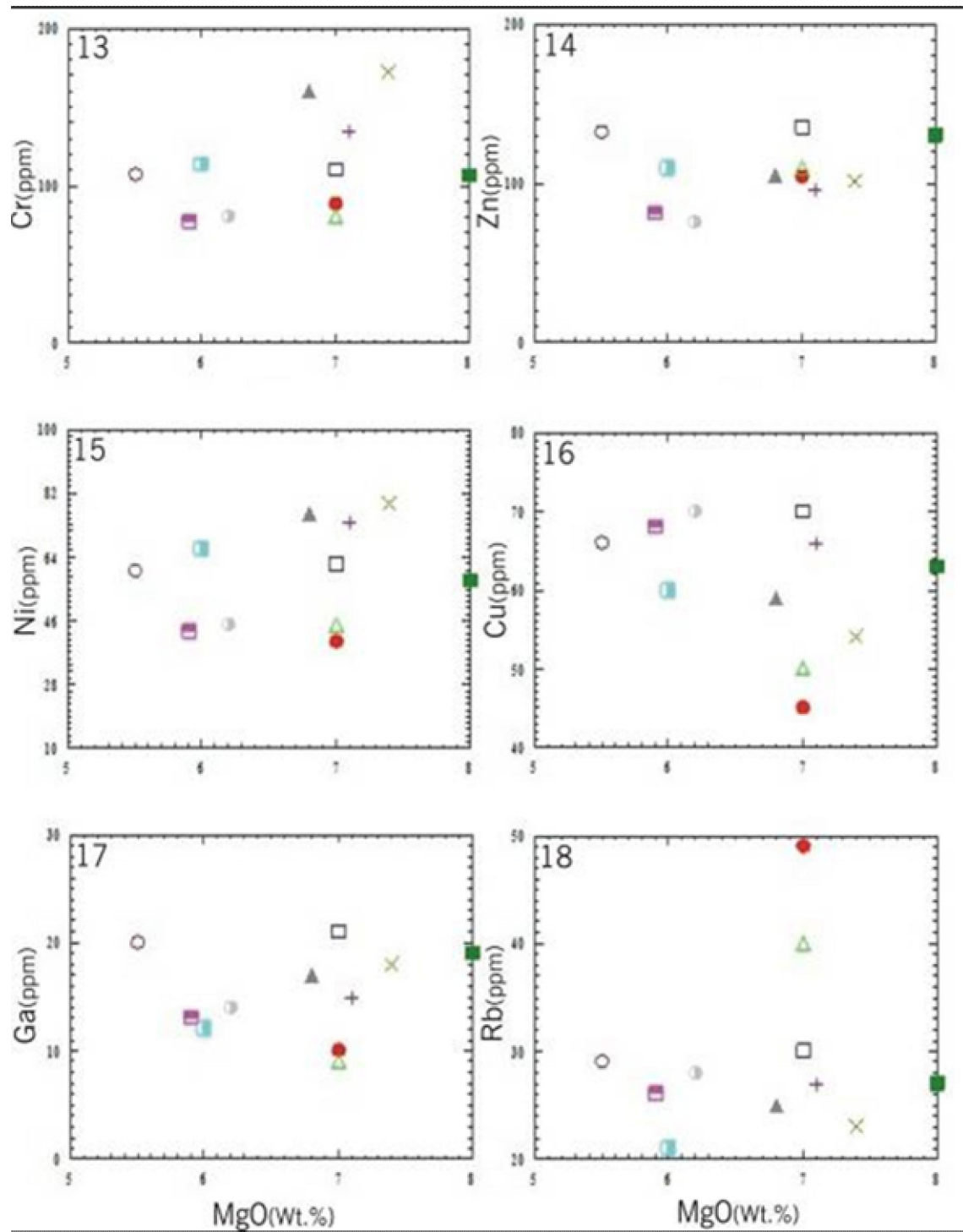
Fig.11. MgO variation diagrams of the studied basaltic samples: (13) Cr, (14) Zn, (15) Ni, (16) Cu, (17) Ga, (18) Rb. Symbols as in Figure (9).
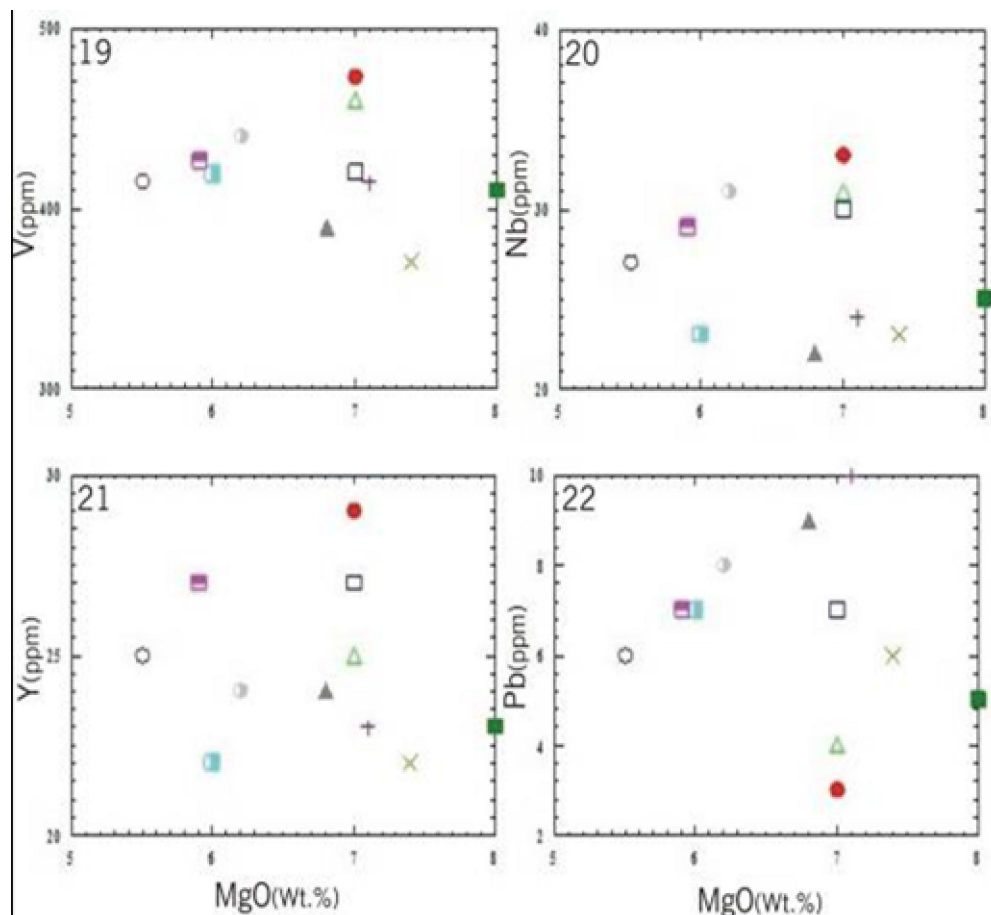
Fig.12. MgO variation diagrams of the studied basaltic samples: (19) V, (20) Nb, (21) Y, (22) Pb. Symbols as in Figure (9).

5.5. Tholeiitic-alkaline affinity of the studied lava flow

The **tholeiitic** lava flow of Al-Hemmah (Samples **1**, **4**, **5** & **6**) and Resan Ikteifa (Samples **9**, **10** & **11**) are commonly mountains and always uniform chemical composition for several kilometers. The characteristic chemical traits are high TiO_2 (2.6-3.8%), low MgO (5.5-7.4%), and high Ni (43-79ppm), Zn (75-132ppm), Zr (106-130ppm), Ba (718-950ppm), Sr (639-795ppm), V (370-440ppm), and Cr (77-172ppm). The flow is generally approximately undersaturated with silica (46.5-48%) and with normal contents of Al_2O_3 (12.3-14.5%). According to **Carmichael *et al.* (1974)** the normal content of Al_2O_3 of most continental tholeiitic magma is between 13% and 15.5% (Table 1). The olivine content of these samples varies from 1.41 to 14.1 and according to the preferred nomenclature would be classified as olivine-bearing tholeiitic basalt. The anorthite plagioclase content varies from 17.78 to 24.67% (Table 2). The final clinopyroxene is determined as diopside and it varies from 11.82 to 24.64%. The determination of hypersthene is not needed in the pure volcanic facies

because all hy will enter the clinopyroxene. The accessory minerals include magnetite, ilmenite and apatite. Ilmenite ranges between 4.89 and 7.15%, whereas magnetite and apatite are distributed from 2.46 to 2.73% and 0.95 to 1.49%, respectively. The total amount of normative accessory minerals corresponds to the modal content of the opaque constituents.

The **alkali** basalts of Al-Hemmah (Sample **2** & **3**) and Resan Ikteifa (Sample **7** & **8**) flows are undersaturated basalts which always contain normative nepheline (0.5-1.39). Another characteristic feature is the high content of normative olivine (13.96-19.81) and low content of pyroxene (Di=17.72-25.41). There is also a single pyroxene phase which is chemically identified as diopside. Chemically, the alkali basalts are recognizable higher in alkalis (Na_2O, 2.8-3.1%; K_2O, 0.9-1.2%) and considerable lower in silica (SiO_2, 45.2-46.5%) than the tholeiitic basalts (Table 1).

Hypersthene can not form in the alkali basalts because all Hy will be desilicated to form olivine. For the same reason the clinopyroxene appears to be rich

in CaO. Its content in Fe$_2$O$_3$, on the other hand is generally low. The alkali basalts of the Al-Hemmah and Resan Ikteifa differ geochemically from the tholeiitic basalts by the common detection of higher concentrations of Ba (890-1053ppm), Sr (715-909ppm) and Zr (120-151ppm) and low concentrations of Cr (80-110ppm). The elements Cu, Ga, Y, Nb, Pb and Rb show nearly similar values in both types of basalts (Table 1).
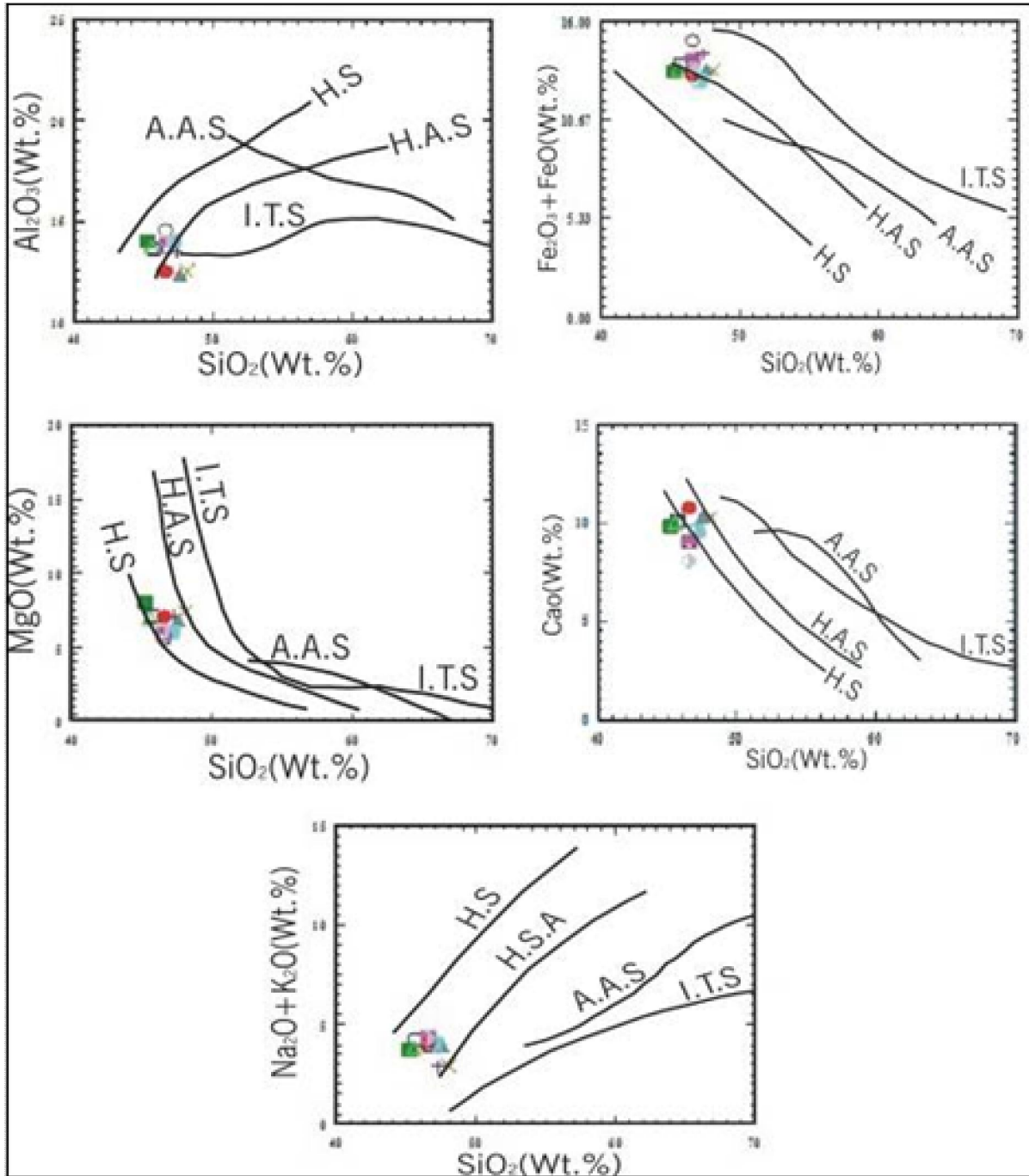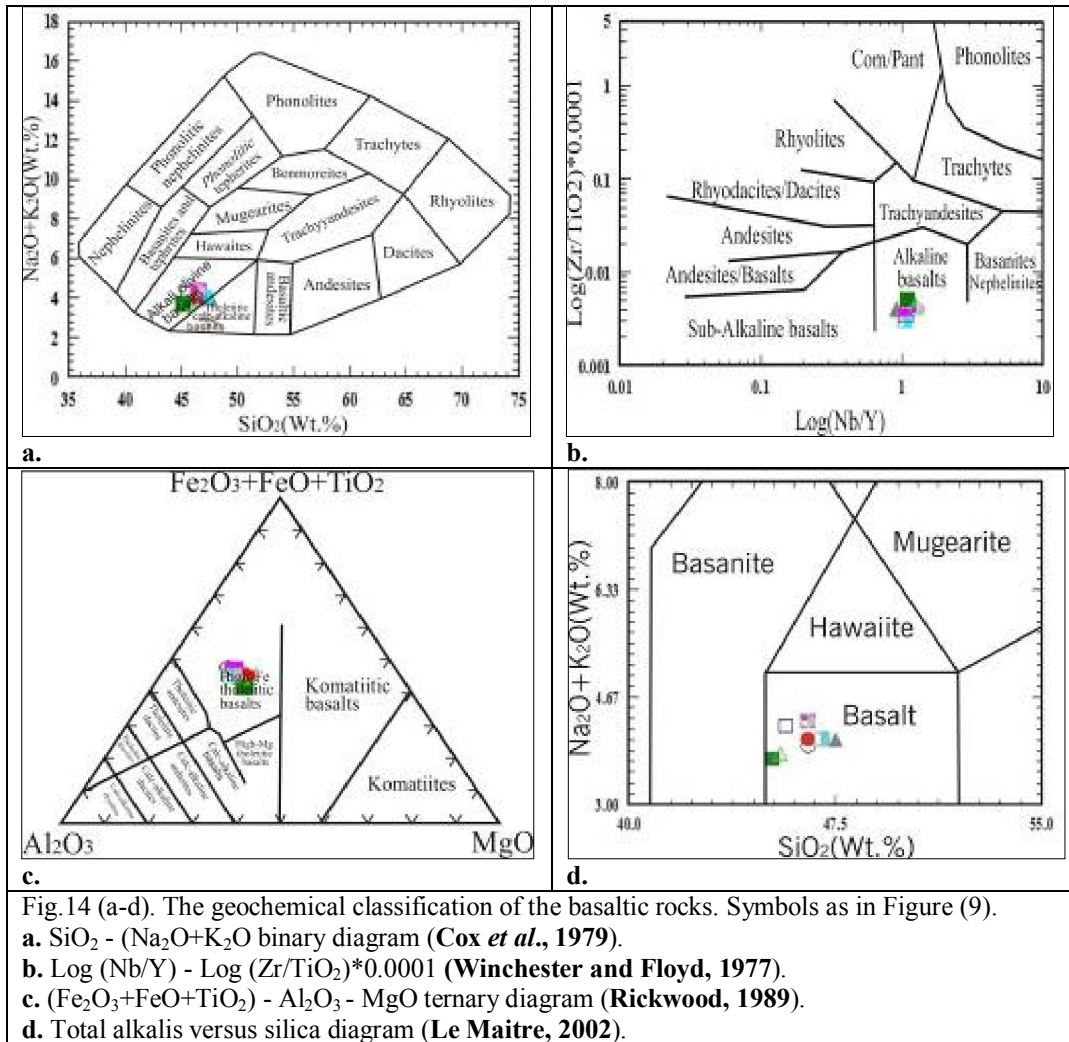

Fig.13. Plot of the studied basalts in comparison with magmatic differentiation trends of hyper alkaline suite of Ross Island and Antractica, (H.S), Hawaiian alkaline suite (H.A.S), Aleutian orogenic andesite suite (A.A.S) and Icelandic tholeiitic suite (I.T.S; **Middlemost, 1985**). Symbols as in Figure (9).

Fig.14 (a-d). The geochemical classification of the basaltic rocks. Symbols as in Figure (9).
a. SiO$_2$ - (Na$_2$O+K$_2$O binary diagram (**Cox** *et al.*, **1979**).
b. Log (Nb/Y) - Log (Zr/TiO$_2$)*0.0001 (**Winchester and Floyd, 1977**).
c. (Fe$_2$O$_3$+FeO+TiO$_2$) - Al$_2$O$_3$ - MgO ternary diagram (**Rickwood, 1989**).
d. Total alkalis versus silica diagram (**Le Maitre, 2002**).

5.6. Tectonic environment and crust evolution

In the continental areas of the Earth, basaltic volcanism is often found in areas of tectonic tension and rifting such as north Red Sea rifting. Extensional tectonic activity may result in the eruption of continental flood basalts, as has already been noted in north Sinai. However, the rifting of continental crust is associated with the emplacement and eruption of a very wide range of different igneous rocks. Structural basins and north Red Sea rifting may also develop within a continent as the result of continent-continent collision such as the East African rift system. Continental rift are dominated by alkalic rocks and contain mainly tholeiitic basalts (**Middlemost, 1985**).

Contemporaneous with the first stage of the Red Sea spreading (**Almond, 1986**), a major period of continental flood basalt took place in Ethiopia and Yemen (**Zanettin** *et al.*, **1980** and **Mohr, 1987**), as well as basalt flows and dykes in the Eastern and Western Deserts and Sinai (**Steinitz** *et al.*, **1978**; **Abdel-Monem and Heikel, 1981**; **Abdel Aal, 1988**;

Saleeb Roufaiel *et al.*, **1989**; **El-Desoky** *et al.*, **2015**). Volcanic eruptions and flow activities of Oligocene Miocene are synchronous with the opening of the Red Sea (**Harland** *et al.*, **1982** and **El-Desoky** *et al.*, **2015**).

Tectonic environment for the formation of these basalts may be implied by trace elements, in particular by incompatible high field strength elements (such as Nb, Ta, Zr, Hf, Ti, and Y).

Basaltic magma occurred in intraplate setting is usually enriched in high field strength elements, while basaltic magma which was contaminated by crust, or formed in subduction zone environment is usually enriched in large ion lithophile elements. Thus, if basalt in within plate tectonic setting came from the enriched mantle or had been contaminated by crust, high field strength elements and large ion lithophile elements may be rich (**Edwards** *et al.*, **1991**).

The tectonic environments are distinguished on the Zr/Y versus Zr binary diagram (Fig.17a) of **Pearce and Norry (1979)** the studied samples fall in

within-plate basalts. A discrimination diagram using the TiO$_2$ versus Zr has been proposed by **Pearce and Cann (1973)**. Appling the data of the examined samples, all plots fall as cluster in the field of within-plate basalts (Fig.17b). In the tectonic discrimination diagram (Fig.17c) of the Nb*2-Zr/4-Y plot of **Meschede (1986)** these studied samples fall in within-plate tholeiite.

6. Petrogenesis

The normalized spidergrams are used to facilitate the comparison of the distribution of incompatible elements in a group of rocks. A comparison of the distribution of these elements in the studied basaltic samples with reference to some international values of chondrite, oceanic island basalt (OIB), N-MORB and E-MORB are presented (Fig.18a-d). From these diagrams it is inferred that there is a good agreement between the studied basaltic samples and N-MRB and E-MORB.

Content on the trace element patterns of studied basalt are show relatively enriched of Zn, Zr and Cr which characterizes the tholeiitic rocks.

A multistage process is recommended for the origin of these rocks. In this model, partial melting of amphibolite formed from the basaltic crust of the down-going oceanic slab, rise and interact with the overlying asthenospheric mantle wedge to produce the early tholeiitic melt. The later stage as possible further was modified by shallow fractional crystallization (**Lopez-Escoloar et al., 1977**).

The samples show a negative correlation with Fe enrichment suggesting that significant crustal contamination. High content of Fe$_2$O$_3$ and MgO also suggest that considerable crustal contaminations (**Arndt and Jenner, 1986**). The low CaO/Al$_2$O$_3$ ratio value in the samples suggests that amphibole was not involved during the generation on this magma (Table 3).

Basalts from the Oslo rift have major and trace element contents similar to those of oceanic island basalts (OIB), supporting the involvement of asthenospheric mantle in their origin (**Neumann et al., 1990**). However, trace element abundances in studied basalt characterize rocks derived from enriched subcontinental lithospheric mantle (Fig.19c) and rule out asthenospheric mantle source in true continental rift environments.

7. Source and fractionation

Although differences in the degree of melting of mantle peridotite can lead to variations of TiO$_2$ content in basalt, the basaltic magma from the asthenosphere generally has a relatively high Ti content (average value of TiO$_2$ in OIB's is 2.86%), while Ti content of basaltic magma from the lithosphere mantle is relatively low (**Ewart et al.,**

1998). High TiO$_2$ content in volcanic rocks (2.4%–3.8%) mainly comes from the asthenosphere mantle. All samples have steep HREE distribution patterns (Fig.18a-d), which indicate that the magma comes from a single garnet mantle (**Edwards et al., 1991**).

The magmatic evolution is related to the processes of fractional crystallization. It is confirmed by the behavior of some of the compatible elements Fe, Ti, Mg, and Ca displaying trends of decreasing with the magmatic evolution.

The Y-Zr relationship (Fig.19b) indicates a little enrichment in Zr with an insignificant increase in Y. This feature cannot explain a mineral phase controlling Y. It is suggested that the residual mineralogy of the mantle source is responsible for the poorly developed Y enrichment (**Nesbitt and sun, 1976**).

Vanadium is compared with the incompatible element Zr (Fig.19c). According to **Nesbitt and Sun (1976)**, the V/Zr ratio for the low-MgO basalt is 3%. In the studied samples the ratio varies between 3.17 and 3.95 (Table 1).

The small scatter of studied basaltic samples (Fig.9 & 12) suggests a close genetic affinity. These samples are interpreted as having developed at high pressure, within the upper mantle, with little or fractionation in the upper parts of crust (**Thompson et al., 1972**). **Nesbitt and Sun (1976)** suggested that basalts with MgO content between 5.5% and 8% are differentiation products of MgO-rich magma but originated from a primary source with 12% MgO.

The basalt is confirmed by the behavior of some of the compatible elements Fe, Ti, Mg, and Ca displaying trends of decreasing with the magmatic evolution. The decrease of Fe and Ti owes to fractionation of titanomagnetite in combination with other mafic minerals (pyroxenes and amphiboles), whereas Ca and Mg decrease as a result of crystallization of amphibole, clinopyroxene and partly plagioclase.

Some trace elements such as Cr, Ni, V, Sr, Zr, and Y also display similar trends. The decrease of Cr and Ni content could be related to the fractionation of olivine, clinopyroxene and spinel, while V has relation to Fe-Ti oxides. The diminishing of Na and Y content, well presented in Al-Hemmah-Resan Ikteifa, could be ascribed to the fractionation of amphibole. This is confirmed by the presence of amphibole xenoliths incorporated in subvolcanic bodies from the Al-Hemmah-Resan Ikteifa volcanics.

The decreases of P content with the magmatic evolution in Al-Hemmah-Resan Ikteifa tholeiitic basalt due to the fractionation of apatite. The decreasing of K with SiO$_2$ increasing could be explained only with a fractionation of potassic mineral

phase that could crystallize early in water rich primitive melts.

The specific trends of MgO and CaO increasing with magmatic evolution for Al-Hemmah-Resan Ikteifa contradict the tendencies explained by the fractionation of mafic minerals. These specific trends could be explained if we allow simultaneous to the fractionation, intensive fluid assisted melting of clinopyroxenites at greater depth.
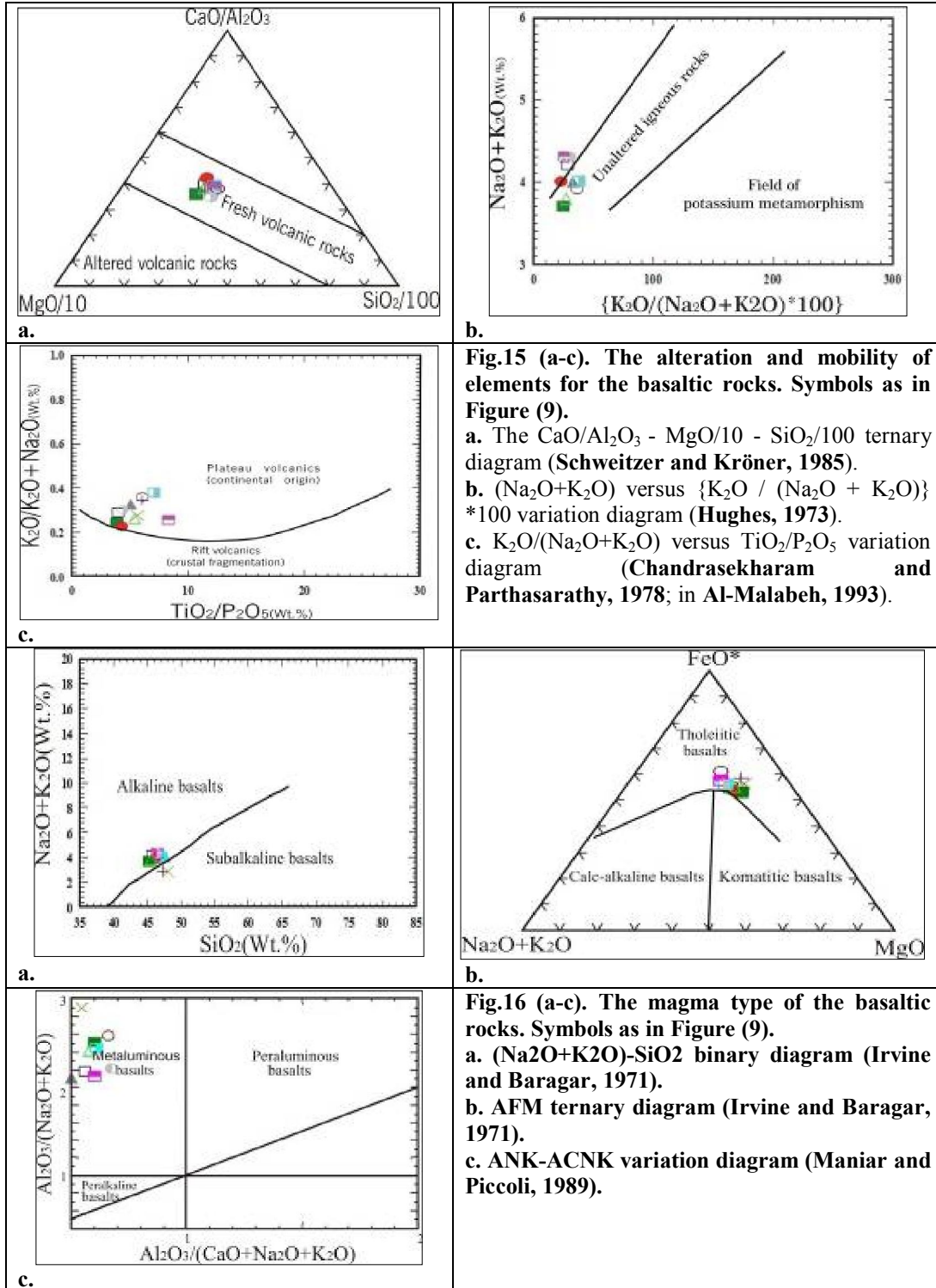

a.

b.

Fig.15 (a-c). The alteration and mobility of elements for the basaltic rocks. Symbols as in Figure (9).
a. The CaO/Al$_2$O$_3$ - MgO/10 - SiO$_2$/100 ternary diagram (**Schweitzer and Kröner, 1985**).
b. (Na$_2$O+K$_2$O) versus {K$_2$O / (Na$_2$O + K$_2$O)} *100 variation diagram (**Hughes, 1973**).
c. K$_2$O/(Na$_2$O+K$_2$O) versus TiO$_2$/P$_2$O$_5$ variation diagram (**Chandrasekharam and Parthasarathy, 1978**; in **Al-Malabeh, 1993**).

c.

a.

b.

Fig.16 (a-c). The magma type of the basaltic rocks. Symbols as in Figure (9).
a. (Na2O+K2O)-SiO2 binary diagram (Irvine and Baragar, 1971).
b. AFM ternary diagram (Irvine and Baragar, 1971).
c. ANK-ACNK variation diagram (Maniar and Piccoli, 1989).
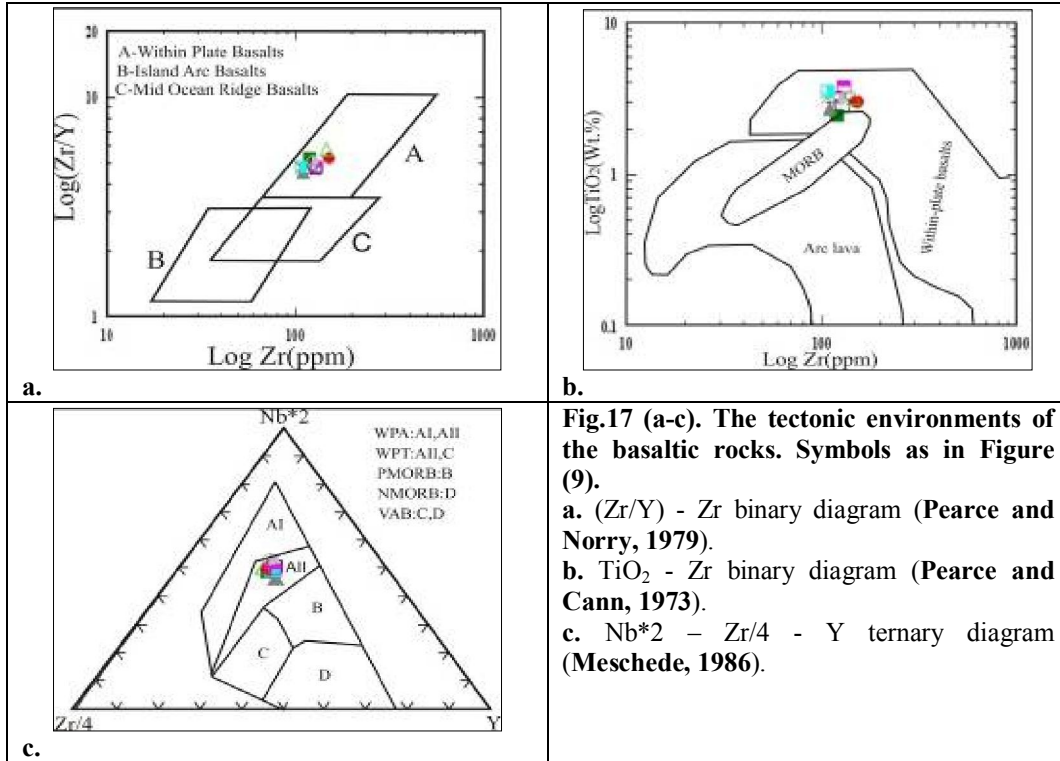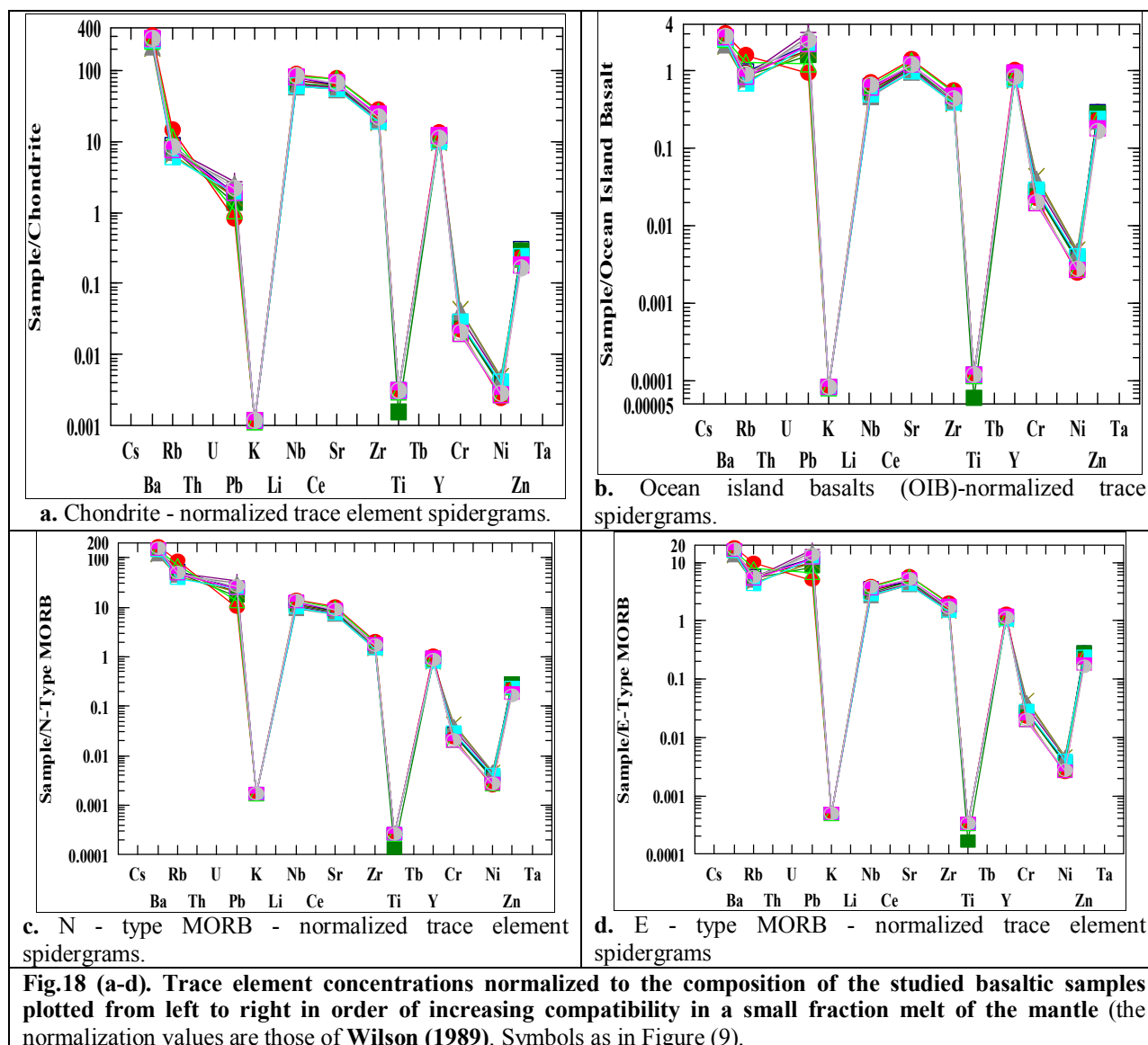
c.

a.

b.

c.

Fig.17 (a-c). The tectonic environments of the basaltic rocks. Symbols as in Figure (9).
a. (Zr/Y) - Zr binary diagram (**Pearce and Norry, 1979**).
b. TiO_2 - Zr binary diagram (**Pearce and Cann, 1973**).
c. Nb*2 – Zr/4 - Y ternary diagram (**Meschede, 1986**).

Table 5. The averages chemical composition of major, minor and trace elements for W, Q and M compared to published data by Wilson (1989).

Oxides	W	Q	M	OIB	N- MORB	E- MORB
SiO_2	50.88	50.25	47.48	50.75	50.40	51.18
TiO_2	0.23	0.26	1.35	13.41	15.19	16.01
Al_2O_3	16.20	16.50	15.68	3.62	1.36	1.69
Fe_2O_3	7.19	7.30	6.87	13.63	10.01	9.40
FeO	4.25	4.28	7.64	--	--	--
MnO	--	--	--	0.18	0.18	0.16
MgO	6.28	6.59	5.55	9.60	11.43	11.49
CaO	7.29	7.36	7.80	5.25	8.96	6.90
Na_2O	3.30	2.63	5.15	0.77	0.09	0.43
K_2O	1.88	1.50	0.53	2.80	2.30	2.74
P_2O_5	0.08	0.16	0.08	0.42	0.14	0.15
LOI	1.60	1.08	0.35	--	--	--
Trace elements (ppm)						
Cr	24.25	522.75	115.75	81	346	225
Ni	7.25	140.5	113.5	78	177	132
Cu	16.75	153.75	24	--	--	--
Zn	110.75	156.5	189.75	--	--	--
Zr	188.5	153.5	177	227	--	--
Rb	273.75	221.25	81.5	--	--	--
Y	57.25	54	1.75	42	37	39
Ba	57	345.25	172.75	191	<20	86
Pb	37.75	8.75	4.25	--	--	--
Sr	3.50	115.75	144.75	395	98	155
Ga	25	37.5	17	--	--	--
V	2	270.75	312	--	--	--
La	--	--	--	24	2.95	6.92
Ce	--	--	--	53	12	17.80
Nb	13.75	7.5	233.75	21.5	2.10	8.60

a. Chondrite - normalized trace element spidergrams.

b. Ocean island basalts (OIB)-normalized trace spidergrams.

c. N - type MORB - normalized trace element spidergrams.

d. E - type MORB - normalized trace element spidergrams

Fig.18 (a-d). Trace element concentrations normalized to the composition of the studied basaltic samples plotted from left to right in order of increasing compatibility in a small fraction melt of the mantle (the normalization values are those of **Wilson (1989)**. Symbols as in Figure (9).

Discussion and conclusion

Sinai Peninsula lies in the northern part of Egypt, between the Gulfs of Suez and Aqaba at the southern end, and the Mediterranean Sea at the northern end. This region is considered to be an active seismic area due to the presence of the triple junction of the Gulfs of Suez and Aqaba and the Red Sea (**Khalil, 1998**).

The Red Sea Rift forms an elongated, northwest striking depression with a length of approximately 2000 km.

It separates the African Plate from the Arabian Plate as part of the entire rift system that includes the Gulf of Aden, the East African Rift, the Gulf of Suez and the Gulf of Aqaba. With the initiation of this rift system in the Oligocene to Early Miocene, the former continuous Afro-Arabian shield was fragmented and split into the African and Arabian Plates (**Martinez**

and Cochran, 1988). A major stage of the rifting process occurred in the Early to Middle Miocene, when the opening of the Red Sea was compensated in the north no longer by the Suez Rift but by the sinistral Dead Sea Transform. The onset of the transform motion started about 20 Ma ago (**Girdler, 1985**; **Joffe and Garfunkel, 1987**).

Ocean deeps are widespread features within the Red Sea; their formation is thought to be a first sign documenting the transition from continental rifting to sea floor spreading (**Bonatti, 1985**; **Martinez and Cochran, 1988**; **Cochran and Martinez, 1988**). The Red Sea Rift makes, as part of the African-Arabian rift system, a good location to study the evolution from continental rifting to sea floor spreading. Whereas the southern part of the Red Sea exhibits already organized sea floor spreading since 5 Ma

(**Röser, 1975**), the northern part is thought to be in the late stage of continental rifting (**Martinez and Cochran, 1988**). The central part is in an intermediate stage (Fig.20; **Searle and Ross, 1975**).
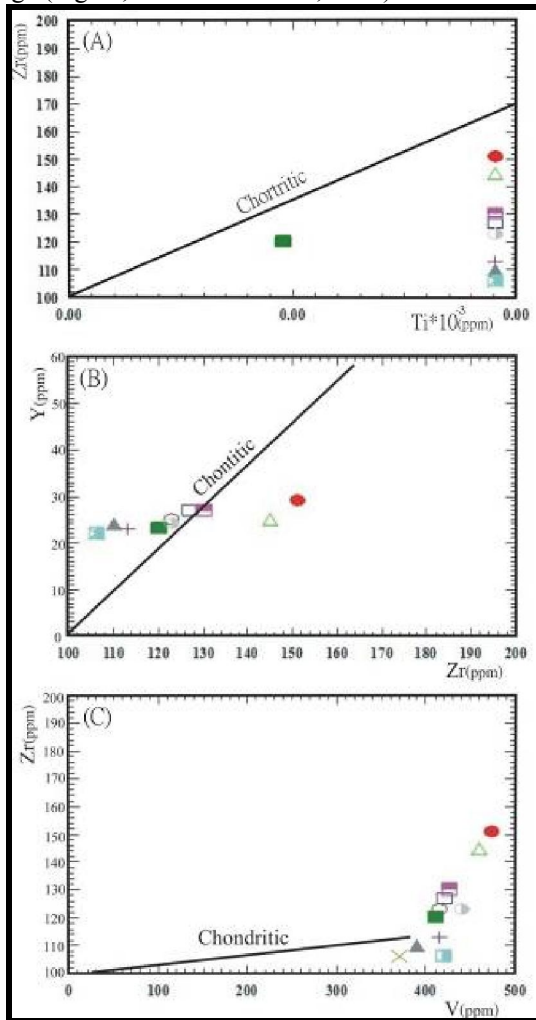

Fig.19. A. (Zr - Ti), B. (Y - Zr), C. (Zr - V) variation diagrams (**Nesbitt and Sun, 1976**) shows the chondritic ratio and the distribution of the studied basalts. Symbols as in Figure (9).

Periodical reactivation of Precambrian fracture systems throughout the Phanerozoic supplied conduit for different types of plutonic and volcanic rock assemblages (**Meneisy, 1990**). During the Late Eocene (41 Ma) to Recent, magmatic activity became widespread on a regional scale occurrences formed in North Africa (**Wilson and Guiraud, 1998**). These occurrences reflect a change in the plate tectonic regime induced by the Alpine collision. They are associated with the opening of the Red Sea and the Gulf of Suez, and with domal uplifts of the basement rocks.

Tertiary basaltic rocks are widely distributed north of Latitude 28°N in Egypt (**Tawadros, 2012**).

Basaltic rocks also cover a large area beneath the Nile Delta and adjacent parts of the Western Desert. In Sinai, several minor Tertiary basaltic outcrops occur. Tertiary basaltic rocks occur mainly in the form of sheets, dikes, and sills. The basalts of the Abu Zaabal, Abu Rawash, and Gabal Qatrani are doleritic basalts. Volcanics of the Gabal Qatrani overlie the sandstones of the lower Oligocene Gabal Qatrani Formation and they are overlain by the lower Miocene Khashab sandstones. They are composed predominantly of amygdaloidal, altered, olivine basalts, which represent tholeiitic transitional-continental within plate basalts (**El-Bayoumi et al., 1997**).

Basaltic dikes from the Southern Western Desert gave ages around 40 Ma (**Meneisy and Kreuzer, 1974**). Volcanic activities related to the opening of the Red Sea took place in a series of successive pulses ranging in age from the Late Oligocene to the Middle Miocene. The Ragabat El-Naam dike trends E-W parallel to a large fault belonging to the Central Sinai-Negev Shear zone. It gave an isochron age around 25 Ma (Upper Oligocene; **Steinitz et al., 1978**).

The studied basaltic rocks occur as sheets capping the hills as well as minor sills intruding the Tertiary sediments. Vertical columnar jointing is observed. Two basaltic exposures crop out at Al-Hemmah in an E-W and NE-SW trends along a distance of 3km and 1km respectively. It seems probable that they are localized along a fault forming a fault scarp. The volcanic regions vary in volume from large volcanoes (Al-Hemmah), to small isolated sheets and sills (Resan Ikteifa).

The alkali basalts developed in Al-Hemmah-Resan Ikteifa is characterized by low silica and high alkali (sodium-rich) and iron titanium contents. The alkali basalts from Al-Hemmah-Resan Ikteifa were formed in the Red Sea rift setting of continent stretching environment. It is the product of rapid rising of the melt derived from tension partial melting of phlogopite-amphibole bearing material from asthenospheric mantle. The primary magma has not been contaminated significantly by crust materials.

The major oxides and trace elements characteristics of the most primitive mafic magmatic rocks (MgO $\geq$ 6 wt %) provide important constraints on the nature of the mantle source and the conditions of partial melting. These are predominantly sodic (alkali olivine basalts). The sodic magmas were derived by variable degrees of partial melting within a transitional zone between garnet-peridotite and spinel-peridotite mantle facies, close to the base of the lithosphere. Mantle partial melting was induced by adiabatic decompression of the asthenosphere, locally in small-scale, plume-like, diapirs which appear to upwell from ~ 400 km depth.
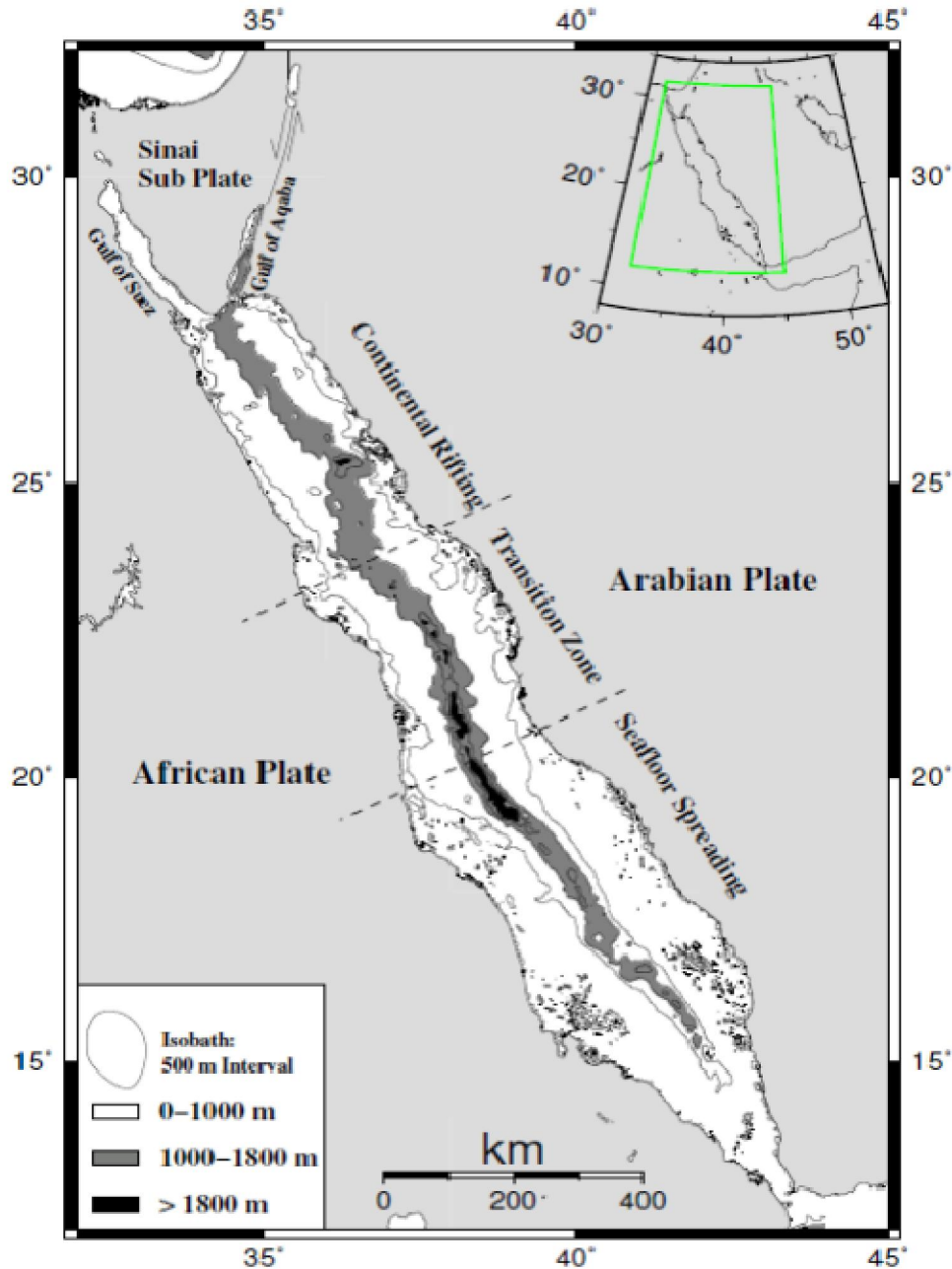
Fig.20. The Red Sea can be separated into three parts along strike. The southern part is characterized by organized sea floor spreading. The central part in a transition zone between continental rifting and sea floor spreading. The northern part shows no sign of spreading. The grey shaded area comprises water depths of more than 1000m and images the axial trough and axial depression, respectively (**Smith and Sandwell, 1997**).

The rupturing process propelled the newly evolved Arabian Plate away from Africa is in a northwesterly direction. The stresses released after rupturing processes gave rise to linear zones of crustal weakness and high heat flow and along these northwestern-southeastern trending weak zones, the magmatism of North Africa suite was triggered by mantle plume. Fixed mantle plumes are considered to burn through lithospheric plate giving rise to localized igneous activity. Where lithosphere is continental, the activity is represented by alkaline magmatism including subalkaline sub volcanic complexes.

and Al-Azhar University for constructive comments and fruitful discussion and we thank the associate Prof. Ibrahim Hashim, Nuclear Material Authority for providing laboratory facility for chemical analyses.

References

1. Abdel Aal, A.Y., 1988. Characteristics and age of the volcanic rocks of South El-Quseir Red Sea Costal Plain, Egypt. J. Geol., V. 32, pp. 27-48.
2. Abdel Aal, A., Day, R.A., Lelek, J.J., 1992. Structural evolution and styles of the northern Sinai, Egypt. Proceedings of 11th Egyptian General Petroleum. Corporation Exploration and Production Conference, Cairo, 1, 546–562.
3. Abdel-Meguid, A.A., 1992. Late Proterozoic Pan African tectonic evolution of the Egyptian part of the Arabian-Nubian Shield. Middle East Research Center (M.E.R.C.) Ain Shams Univ., Cairo, Egypt. Earth Sc Ser 6:13–28.
4. Abdel-Monem, A.A., Heikel, M.A., 1981. Major element composition, magma type and tectonic environment of the Mesozoic to recent basalts, Egypt: A review. Bull. Faci. Earth Sci., K.A.U., Vol. 4, 121- 148p.Faculty of Earth Sciences, King Abdul-Aziz University, Jeddah, Kingdom of Saudi Arabia.
5. Abu El-Enen, M.M., 2001.The contact aureole around a Tertiary dolerite sill, East Gebel Yelleq, Northern Sinai, Egypt. The second international conference on the geology of Africa. Vol. (I), P-P.369-384 (Oct. 2001) Assiut, Egypt.
6. Abu El-Leil, I., 1988.Petrogenesis of some Tertiary volcanics, North Sinai, Egypt. Mid East Res. Cent. Earth Sci. Ser, Ain Shams University , Cairo , Egypt, v. 2 ,1988, p. 68-79.
7. Al-Malabeh, A., 1993. The Volcanology, mineralogy and geochemistry of selected pyroclastic cones from NE-Jordan and their evaluation for possible industrial applications. Ph.D. thesis, Erlanger, Germany.
8. Almond, D.C., 1986. The relation of Mesozoic – Cenozoic Volcanism to tectonics in the Afro – Arabian dome. J. Geoth. Res. V. 28, pp. 225-246.
9. Arndt, N.T., Jenner, G.A., 1986. Crustally contaminated komatiites and basalts from Kambalda. Western Ausralia: Chem. Geol. 56, 229-255.
10. Baldridge, W.S., Eyal, Y., Bartov, Y., Steinitz, G., Eyal, M., 1991; Miocene magmatism of Sinai related to the opening of the Red Sea. Tectonophysics, 197: 181-201.
11. Bonatti, E., 1985. Punctiform initiation of seafloor spreading in the Red Sea during transition from a continental to an oceanic rift, Nature, 316, 33-37p.
12. Carmichael, I.S.E., Turner, F.J., Verhoogen, J., 1974. "Igneous Petrology", McGraw-Hill. Inc., New York, 739p.
13. Chandrasekharam, D., Parathasarathy, A., 1978. Geochemical and tectonic studied on the coastal and inland Deccan Trap volcanic and a model for the evolution of Deccan Trap volcanism. N. Jb. Min. Abh., 132, 214-228.
14. Cochran, J., Martinez, F., 1988. Evidence from the northern Red Sea on the transition from continental to oceanic rifting, Tectonophysics, 153, 25-53p.
15. Cochran, J., Martinez, F., Steckler, M.S., Hobart, M.A., 1986. Conrad Deep: a northern Red Sea deep. Origin and implication for continental rifting, Earth and Planetary Science Letters, 78, 18-32p.
16. Courtillot, V., Armijo, R., Tapponnier, P., 1987. Kinematics of the Sinai triple junction and a two phase model of the Arabia-Africa rifting, in Continental Extensional Tectonics from Coward, M.P., Dewey, J.F. and Hancock, P.L. (eds), Geological Society Special Publication No.28, 559-573p.
17. Cox, K.G., Bell, J.D., Pankhurst, R.J., 1979. The Interpretation of Igneous Rocks. London (George Allen & Unwin), 1979. xiv + 450 pp., 197.
18. Edwards, C., Menzies, M., Thirlwall, M., 1991. Evidence from Muriah, Indonesia, for the interplay of supra-subduction zone and intraplate processes in the genesis of potassic alkaline magmas [J]. *Journal of Petrology*. 32, 555–592.
19. EGPS, 1993a. Geological map of Gabal Libni Quadrangle Sinai- Egypt.
20. EGPS, 1993b. Geological map of Al-Hasanah Quadrangle Sinai- Egypt.
21. El-Bayoumi, R.M., Abu Zeid, H.T., Khalaf, E.A., 1997. Upper Proterozoic calc-alkaline and tholeiitic volcanics and their associates in the Gulf of Suez region, Egypt. Ann. Geol. Surv. Egypt 20, 125–142p.
22. El-Desoky, H.M., Khalil, A.E., Afifi, A.A., 2015. Geochemical and petrological characteristics of the high-Fe basalts from the Northern Eastern Desert, Egypt: Abrupt transition from tholeiitic to mildly alkaline flow-derived basalts. Nature and Science 2015; 13(6).
23. El-Sayed, M.K.A., 2012. Palaeomagnetic Investigations of the Volcanic Intrusion at Bir Al-Hemmah Area, North Central Sinai, Egypt. Australian Journal of Basic and Applied Sciences, 6(8): p. 609-617.
24. Ewart, A., Milner, S.C., Armstrong, R.A., Dungan, A.R., 1998. Etendeka volcanism of the Goboboseb Mountains and Messum igneous

complex, Namibia. Part I: Geochemical evidence of Early Cretaceous Tristan Plume Melts and the role of crustal contamination in the Paraná–Etendeka CFB [J]. *Journal of Petrology.* 39, 191–225.

25. Farag, I.A.M. and A. P. Shata. 1954. Detailed geologic survey of El-Minsherah area. Bulletin de l'Institut du Désert d'Egypte 4, n. 2:5–82.

26. Garfunkel, Z., 1981. Internal structure of the Dead Sea leaky transform (rift) in relation to plate kinematics, Tectonophysics, 80, 81-108p.

27. Gass, I.G., 1970.Tectonic and magmatic evolution of the Afro-Arabian dome. In Clifford, T.M. and Gass, I.G. African magmatism and tectonics, Oliverand, Boyd, Edinburgh, 285-300.

28. Geological Survey of Egypt, 1992. Geological map of Sinai, Arab Republic of Egypt. Sheet No. 5, scale 1: 250 000.

29. Girdler, R.W., 1985. Problems concerning the evolution of oceanic lithosphere in the northern Red Sea, Tectonophysics, 116, 109-122p.

30. Harland, W.B., Cox, A.V., Lewellyn, P.G., Pickton, C.A., Walters, R., 1982. A geologic time scale. Cambridge Earth Sci, Ser., 131.

31. Hughes, G.J., 1973. Spilites, Keratophyres and the igneous spectrum. Geol. Mag. 109, 513-527.

32. Hume, W.F., 1962. Geology of Egypt .v.III The stratigraphical history of Egypt, part I from the close the Precambrian episodes to the Cretaceous period, Cairo, Government Printing Offices. p.721.

33. Ibrahim, E.H., Odah, H.H., El-Agami, N.L., Abu El-Enen, M., 2000. Paleomagnetic and geological investigation into southern Sinai volcanic rocks and the rifting of the Gulf of Suez. Tectonophysics, 321: 343-358.

34. Irvine, T.N., and Baragar, W.R.A., 1971. A guide to the chemical classification of the common volcanic rocks ,Canada. J. Earth. Sci., 8,523-548.

35. Issawi, B., El-Hinnawi, M., Francis, M., Mazhar, A., 1999. The Phanerozoic geology of Egypt: A geodynamic approach. The Egyptian Geological Survey, special publication N. 76.

36. Jenkins, D.A., 1990. North and Central Sinai. In: Said, R. (ed.): the Geology of Egypt, 361-380. Balkema, Roterdam, Brookfield.

37. Joffe, S., Garfunkel, Z., 1987. Plate Kinematics of the circum Red Sea - a re-evaluation, Tectonophysics, 141, 5-22p.

38. Khalil, S.M., 1998. Tectonic evolution of the eastern margin of the Gulf of Suez, Egypt. PhD. Thesis, Royal Hollway, University of London, p. 349.

39. Krenkel, E., 1924. Der Syrische Bogen. Centralbl. Mineral. 9: 274-281, 10:301-313.

40. Le Maître, R.W., 2002. Igneous rocks, a classification and glossary of terms. (Recommendations of the International Union of Geological Sciences Subcommission on the Systematics of Igneous Rocks). Cambridge University Press, Cambridge, p 236.

41. Lopez-Escoloar, L., Frey, F.A., Vergara, M., 1977. Andesites and high alumina basalts from the Central-South Chile. Geochemical evidence bearing on their petrogenesis. Contral. Mineral. Petro, 63, 199-228.

42. Lustrino, M., Wilson, M., 2007. The circum-Mediterranean anorogenic Cenozoic igneous province. Earth-Science Reviews 81, 1–65p.

43. MacDonald, G.A., Katsura, A.T., 1964.Chemical composition of some common igneous rocks, J. Petrol., 5, 82-123.

44. Maniar, P.A., Piccoli, P.M., 1989. Tectonic discrimination of granitoids. Ball. Geol. Soc. Am., 101, 635-643.

45. Martinez, F., Cochran, J.R., 1988. Structure and tectonics in the northern Red Sea: catching a continental margin between rifting and drifting, Tectonophysics, 150, 1-32p.

46. Meneisy, M.Y., 1990. Volcanicity - In Said, R (ed), The Geology of Egypt, Rotterdam, Balkema; pp.157-172.

47. Meneisy, M.Y., Kreuzer, H., 1974. Potassium-argon ages of Egyptian basaltic rocks. Geol. Jb. *Hannover*, D9, 21-31p.

48. Meschede, M., 1986. A method of discriminating between different types of mid-ocean ridge basalts and continental tholeiites with the Nb–Zr–Y diagram. Chemical Geology, vol. 56, no. 3-4, pp. 207-218.

49. Middlemost, A.K., 1985. Magmas and magmatic rocks, Longman Inc., New York, 266.

50. Mohr, P.A., 1987. Crustal Contamination in Mafic Sheets: a summary. In: Halls, H.C., Fahrig, W.C. (Eds.), Mafic Dyke Swarms. Special Publication-Geological Association of Canada, vol. 34, pp. 75–80.

51. Moon, F.W., Sadek, H., 1921. Topography and geology of North Sinai, Petrol. Research Ser., Bull.10.

52. Moustafa, A.R., Khalil, M.H., 1990. Structural characteristics and tectonic evolution of North Sinai fold belts. In: Said, R. (ed.): the Geology of Egypt, 361-380. Balkema, Roterdam, Brookfield.

53. Moustafa, R.A., Khalil, S.M., 1995. Rejuvenation of the Tethyan passive continental margin of north Sinai: deformation style and age (Gebel Yelleg area). Tectonophysics, 241:225-238.

54. Musa, H.E., 1987. Geological studies and genetic correlation of the fluid phase during high grade

metamorphism. Contrib. Mineral. Petrol., 108: 219-240.

55. Mysen, B.O., Kushiro, I., 1977. Compositional variations of coexisting phases with degree of partial melting of peridotite in the upper mantle. Am. Mineral. 2, 843-865.

56. Nesbitt, R.W., Sun, S.S., 1976. Geochemistry of Archaean spinifex-texture peridotites and magnesian and low-magnesian tholeiites. Erath Planet. Sci. Letts., Vol. 31, p. 433-453.

57. Neumann, R.W., Sundvoll, B., Overli, P.E., 1990. A midly depleted upper mantle beneath southeast Norway: evidence from basalts in Permo-Carboniferous Oslo rift. Tectonophysics 178, 89-107.

58. Omran, M.A.B., 1997. Stratigraphical studies of the Upper Cretaceous-Lower Tertiary succession in some localities, Northern Sinai. Ph.D. Thesis, Suez Canal University, 292 pp.

59. Pearce, J.A., Cann, J.R., 1973. Tectonic setting of basic volcanic rocks determined using trace elements analyses. Earth and Planetary Science Letters, 19, 290-300.

60. Pearce, J.A., Norry, M.J., 1979. Petrogenetic implication of Ti, Zr, Y and Nb variations in volcanic rocks. Contrib. Mineral. Petrol. 69,p33-47.

61. Ressetar, R., Nairn, A.E.M., Monrad, J.R., 1981. Two phases of Cretaceous –Tertiary magnetism in the Eastern Desert of Egypt: Palaeomagnetic, chemical and K-Ar evidence. Tectonophysics, 7:193-169.

62. Rickwood, P.C., 1989. Boundary lines within petrologic diagrams, which use oxides of major and minor elements. *Lithos*, 22: 247-263.

63. Röser, H.A., 1975. A detailed geomagnetic survey of the southern Red Sea, Geol. Jahrbuch, 13, 131-153p.

64. Saggerson, E.P., Williams, L.A.J., 1964. Ngurumaite from southern Kenya and its bearing on the origin of the rocks in the Tanganyika alkaline district –J. Petrol., 5,40-81.

65. Saleeb Roufaiel, G.S., Samuel, M.D., Meneisy, M.Y., Moussa, H.E., 1989; K-Ar age determinations of Phanerozoic basalt in west Central Sinai. N.Jb. Geol. Paleont. Mh., V.11. pp. 669-683.

66. Schweitzer, J., Kröner, A., 1985. Geochemistry and petrogenesis of Early Proterozoic intracratonic volcanic rocks of the Venters drop super group, South Africa. Chem. Geol., vol. 51, 265-288.

67. Searle, R.C., Ross, D.A., 1975. A Geophysical Study of the Red Sea Axial Trough between 20.5± and 22±N, Geophysics. J. R. astr. Soc., 43, 555-572p.

68. Smith, W.H.F., Sandwell, D.T., 1997. Global seafloor topography from satellite altimetry and ship depth soundings, Science, v. 277, p. 1957-1962, 26 Sept.

69. Steinitz, G., Nartov, Y., Hunziker, J.C., 1978. K-Ar age determination of some Miocene- Pliocene basalts in Israel, their significance to the tectonics of the rift valley – Geol. Mag., 155,329-340.

70. Tawadros, E.E., 2001. Geology of Egypt and Libya. Balkema, Rotterdam, 468p.

71. Tawadros, E.E., 2012. Geology of North Africa. Taylor and Francis Group, London, 77-79p.

72. Thompson, R.N., Esson, J., Dunham, A. C., 1972. Major elements chemical variation in the Eocene lavas of the Isle of Skye, Scotland. J. Petrol., v. 13, p. 219-253.

73. Williams, H., Turner, F.J., Gilbert, C.M., 1985. Petrography: An introduction of the study of rocks in thin sections. 2nd (ed.), pp. 96-103.

74. Wilson, M., 1989. Igneous petrogenesis. Academic Division of Unwin Hyman, Ltd., London, 466.

75. Wilson, M., Guiraud, R., 1998. Late Permian to Recent magmatic activity on the African-Arabian margin of Tethys. In: Macgregor, D.S., Moody, R.T.J. & Clark-Lowes, D.D. (eds) Petroleum Geology of North Africa. Special Publication of the Geological Society of London No 132, 231-263p.

76. Winchester, T.A., Floyd, P.A., 1977. Geochemical discrimination of different magma series and their differentiations products using immobile elements – Chem. Geol., 20,325-343.

77. Zanettin, B., 1984. Proposed new chemical classification of volcanic rocks –Epis-Odes, 7, 4, 19-20.

78. Zanettin, B., Justin Visentin, E., Nicoletti, M., Piccirillo, E.M., 1980 Correlations among Ethiopian volcanic formations with special references to the chronological and stratigraphical problems of the "Trap Series". Atti Convegni Acc Lincei Roma 47:231–252.

8/25/2016